RESEARCH ACTION ITEM

June 3, 2004 MAIL CONTROL FORM 1:11:03 PM

FROM: M. Podowski, Rensselaer I
TO: C. Paperiello, Dir RES
FOIA#:

RES#: **2004223**
EDO#:
WITS#:

DESCRIPTION: NRC Research Code Development

SPECIAL INSTRUCTIONS: Have incoming scanned into ADAMS

DOCUMENT DATE: May 21, 2004
DUE TO RES: **June 29, 2004**

RECEIVED BY RES: June 2, 2004
DUE TO EDO:

ASSIGNED TO: **F. Eltawila, Dir DSARE** FOR SIGNATURE OF: **C. Paperiello, Dir RES**

COPIES TO:
ROUTING
TClark

MILESTONES:	ORIGINAL DUE	CURRENT DUE	COMPLETED
To RES	06/29/2004		

printed by ATMS 2000, the RES action tracking system

Routing to:

☐ _____ ☐ _____ TClark - Enter in ATMIS; send copy to responsible division.

☐ Flory - Forward to T. Clark

CONTROLLED CORRESPONDENCE
RES FRONT OFFICE REVIEW

ACTION: Put in ADAMS

WITS/GREEN TICKET #: _____ DUE DATE: ~~6/29~~

ASSIGN TO: ☑ DSARE ☐ DRAA ☐ DET ☐ PMDA ☐ F.O. ☐ ODTA

CONCUR WITH: ☐ NRR ☐ NMSS ☐ OGC ☐ CFO ☐ CIO ☐ ____ ☐ ____

MEET EARLY TO RESOLVE ISSUES WITH CONCURRING OFFICES? ☐ YES ☐ NO

	To Be Reviewed by:	Signature Block:	To Be Signed by:
C. Paperiello	☑	☐	☑
J. Craig	☑	☐	☐
M. Lee	☑	☐	☐

DATE DUE TO F.O.: 6/29

F.O. GUIDANCE: ☐ None. Specify:

Rensselaer

Michael Z. Podowski
Professor of Nuclear Engineering & Engineering Physics
Director, Center for Multiphase Research

May 21, 2004

Dr. Carl J. Paperiello
Director, Office of Nuclear Regulatory Research
U.S. Nuclear Regulatory Commission
Washington, DC 20555

Dear Dr. Paperiello:

In case you do not know who I am, I will start with a few pieces of personal information:

- In the past, I was involved in reviewing several NRC-sponsored projects as a member of various expert review panels.
- More recently, I directed the first NRC-sponsored project, exploring the potential benefits to NRC of using multidimensional computational fluid dynamics (CFD) models and methods of reactor thermal-hydraulics for reactor safety applications.
- Currently, we participate, as a subcontractor to Purdue University, in the NRC-sponsored research project under Contract No. NRC-04-03-048, Task Order No. 2, "Two-Phase CFD Enhancements".

For several years, the main thrust of research performed at the RPI Center of Multiphase Research (CMR) has been the development of new mechanistic multidimensional models of multiphase flow and heat transfer, their implementation in several CFD codes (PHOENICS, CFX, FUENT and, currently, NPHASE), development of appropriate numerical methods of solving the governing equations, and model testing. The NRC-sponsored work is a part of a broader research effort, aimed at advancing our knowledge of multiphase flows and developing physically-based models of local interfacial phenomena, for various future applications.

As a part of the research that I have conducted either myself or in collaboration with my colleagues and co-workers, I have run into several issues indicating that some of the models in the current multiphase flow codes, including both commercial CFD codes and one-dimensional system codes, are, to a smaller or higher degree, inconsistent with the basic physics of multiphase flows. In particular, while searching for various reference materials related to the fundamental modeling concepts that I have been working on, I recently examined the model of two-phase pressure loss due to friction that is being used by the NRC system code, RELAP5/MOD3.3. It turns out that this model may result in incorrect results and cause substantial inaccuracies of the predicted reactor system response. A summary of my findings is given in the attached write-up. I am also sending you copies of our recent publications that provide background information about the nature of the problem. Additional results related to the matter of this letter will be published soon.

Department of Mechanical, Aerospace and Nuclear Engineering
Rensselaer Polytechnic Institute • Troy, NY 12180-3590
Tel. (518)276-4000 • Fax (518)276-3055 • email: *podowm@rpi.edu*

Based on my observations and experience to date, I would like to share with you and your colleagues a few thoughts regarding the NRC research on code development. Specifically:

(1) System codes such as RELAP5 or TRAC, and their derivatives, were originally developed several years ago, and some models are based on half-century old technology (see the 1949 paper that I am referring to in my comments). At the same time, those codes are being widely used for reactor safety analyses by both the US NRC and the industry. Furthermore, substantial resources have been dedicated to a further development and upgrading of such codes, apparently focused mainly on numerical advancements, new computer platforms, and code-user interface. In my judgement, it is practically an imperative that the physical models in system codes be revisited and, if necessary, upgraded, so that the reactor safety codes reflect the technology level of the 21-st Century. This issue becomes even more acute when considering future applications of those codes to Generation-IV reactors. I am aware of the fact that the modeling capabilities of various codes have been expanded, but, as the popular saying goes, the weakest link always determines the quality of a chain.

(2) To date, the NRC-sponsored research on the development of advanced multidimensional CFD models and codes has been conducted in a stand-alone fashion, detached from the system code development. Naturally, we have discussed the possibility of linking, in one way or another, the CFD models with the new NRC system code, TRACE-M, that is still under development. Here, I would like to point out potential synergistic effects between the two work areas. Specifically, the development of advanced local multidimensional models has already significantly improved our knowledge of the basic physics of two phase flows. Based on my personal experience, this new expertise can, and should be, used to upgrade the quality of one-dimensional models in the present systems codes and their future upgrades. The issues discussed in the attached write-up are just one example, but I can readily show several other models and situations where the work done at RPI (and elsewhere) would provide useful insight into how to improve, or develop new, simplified 1-D models.

Your response to, and comments on the matter of, this letter will be appreciated.

Sincerely yours,

Michael E. Ishii

c.c. F. Eltawila

Attachment

Comments on the friction pressure drop partitioning model in the RELAP5/MOD3.3 code

Michael Z. Podowski
Center for Multiphase Research, Rensselaer Polytechnic Institute
Email: *podowm@rpi.edu*

1. One-dimensional two-phase flow model formulation

Consider a two-phase gas-liquid flow in a straight tube (or channel) of a constant cross-section area and arbitrary orientation (vertical, inclined or horizontal). The phasic 1-D momentum equations for the liquid and gas phases, respectively, can be written as [1,2,3]

$$\rho_f(1-\alpha)\left(\frac{\partial v_f}{\partial t}+v_f\frac{\partial v_f}{\partial z}\right) = -(1-\alpha)\frac{\partial p}{\partial z}-(1-\alpha)\rho_f g_z - F_f^s + F_{g-f}^i \tag{1}$$

$$\rho_g\alpha\left(\frac{\partial v_g}{\partial t}+v_g\frac{\partial v_g}{\partial z}\right) = -\alpha\frac{\partial p}{\partial z}-\alpha\rho_g g_z - F_g^{Ind} + F_{f-g}^i \tag{2}$$

where F_f^s is the liquid component of the total shear force (wall friction) per unit volume, F_g^{Ind} is the liquid-induced gas component of the total shear force, and $F_{g-f}^i = -F_{f-g}^i = F^i$ is the total gas-to-liquid interfacial force per unit volume. The remaining notation is conventional. Since for most flow regimes, gas is in the form of bubbles (small and spherical or large and distorted), the flow field (and, thus, shear stress) inside the bubbles is not resolved by the model given by Eqs.(1) and (2). Furthermore, especially in vertical channels, bubbles normally do not touch (or have a very limited contact with) the wall, so that the wall friction is mainly between the surface and the liquid phase. This is why the irreversible-pressure-loss-related term in Eq.(2) is called the liquid-induced force. Naturally, by interchanging the roles of the gas and liquid phases, similar equations can be used to model mist flows.

Eqs.(1) and (2) are consistent with Eqs.(3.1-6) and (3.1-7) in the RELAP/MOD3.3 manual [4]. Specifically, the phasic terms corresponding to wall friction are:

$$F_f^s \quad \text{in Eq.(1)} \;\Leftrightarrow\; (\alpha_f\rho_f v_f)\mathrm{FWF} \quad \text{in Eq.(3.1-7) of Ref. 4} \tag{3}$$

$$F_g^{Ind} \quad \text{in Eq.(2)} \;\Leftrightarrow\; (\alpha_g\rho_g v_g)\mathrm{FWG} \quad \text{in Eq.(3.1-6) of Ref. 4} \tag{4}$$

Assuming fully-developed (thus, adiabatic) upward flow conditions in a vertical channel, Eqs.(1) and (2) can be rewritten as

$$-(1-\alpha)\frac{\partial p}{\partial z}-(1-\alpha)\rho_f g - F_f^s + F^i = 0 \tag{5}$$

$$-\alpha\frac{\partial p}{\partial z}-\alpha\rho_g g - F_g^{Ind} - F^i = 0 \tag{6}$$

Eqs.(5) and (6) can be rearranged to obtain

$$F_g^{Ind} = \frac{\alpha}{1-\alpha}F_f^s - \frac{1}{1-\alpha}F^i + \alpha(\rho_f - \rho_g)g \tag{7}$$

$$-\frac{\partial p}{\partial z} - \rho_m g - F_w^s = 0 \tag{8}$$

where

$$F_w^s = F_f^s + F_g^{Ind} = -\left(\frac{\partial p}{\partial z}\right)_{2\phi} \tag{9}$$

is the total two-phase friction pressure gradient, and

$$\rho_m = \rho_f(1-\alpha) + \rho_g\alpha \tag{10}$$

is the mixture density.

Eqs.(7) and (8) can be applied to practically any 1-D fully-developed two-phase flow regime, provided that the appropriate (flow-regime dependent) models of all component-terms are available.

For most two-phase flow regimes (with a few exceptions, such as annular flow), the drag force is the only interfacial force that is important in 1-D models of fully-developed flows. This force is normally determined based on the balance between the drag and net-buoyancy forces

$$F^i = F^D = \alpha(1-\alpha)(\rho_f - \rho_g)g \tag{11}$$

Again, Eq.(11) is consistent with the RELAP/MOD3.3 manual [4].

Using Eqs.(11), Eqs.(7) and (8) yield

$$F_f^s = (1-\alpha)F_w^s = (1-\alpha)\left(-\frac{\partial p}{\partial z} - \rho_m g\right) = -(1-\alpha)\left(\frac{\partial p}{\partial z}\right)_{2\phi} \tag{12}$$

$$F_g^{Ind} = \alpha F_w^s = \alpha\left(-\frac{\partial p}{\partial z} - \rho_m g\right) = -\alpha\left(\frac{\partial p}{\partial z}\right)_{2\phi} \tag{13}$$

On the other hand, the terms in Eqs.(3.1-6) and (3.1-7) of the RELAP5/MOD3.3 manual, that correspond to Eqs.(12) and (13), are given in Ref. 4 by Eqs.(3.3-191) and (3.3-192), respectively, with the term, Z^2, defined by Eq.(3.3-190). Using the current notation (see Eqs.(3) and (4)), Eqs.(3.3-191) and (3.3-192), respectively, become

$$(F_f^s)_{RELAP} = -(1-\alpha)\left(\frac{\partial p}{\partial z}\right)_{2\phi} \frac{Z^2}{\alpha + (1-\alpha)Z^2} \tag{14}$$

$$(F_g^{Ind})_{RELAP} = -\alpha\left(\frac{\partial p}{\partial z}\right)_{2\phi} \frac{1}{\alpha + (1-\alpha)Z^2} \tag{15}$$

Actually, it should be noted that, among several apparent inconsistencies and typographical errors found in Ref. 4, the negative signs on the right hand side of Eqs.(3.3-191) and (3.3-192) are missing (or, what is equivalent, it is incorrectly assumed that $\left(\frac{\partial p}{\partial z}\right)_{2\phi} > 0$, whereas the pressure gradient due to friction is always negative).

Let us consider a dispersed (dilute) flow of small bubbles (or particles) in an adiabatic vertical channel. In such case, the only important interfacial force is the drag force, given by

$$F^D = \frac{1}{8} C_D \rho_f |v_g - v_f| (v_g - v_f) A''' \tag{16}$$

where

$$A''' = \frac{6\alpha}{d_b} \tag{17}$$

is the interfacial area density, and

$$C_D = \frac{24}{Re_b}(1 + 0.1 Re_b^{0.75}) \tag{18}$$

is the drag coefficient.

Furthermore, let us assume that the gas is air, the liquid is water, the bubbles are 0.5 mm in diameter, and the average void fraction is 0.1. Thus, substituting Eq.(18) into Eq.(11), the calculated average relative bubble velocity is, $v_r = v_g - v_f \approx 0.055$ m/s.

Now, assuming a liquid flow mass flux of $G = 1000$ kg/m^2-s in a $D = 2$ cm diameter tube, the single-phase friction pressure gradient is

$$\left(\frac{\partial p}{\partial z}\right)_{LO} = -\lambda_f \frac{G^2}{2\rho_f D} = -635 \text{ N/m}^3 \tag{19}$$

where the liquid-only (LO) single-phase friction factor is, $\lambda_f \approx 0.025$.

Since, for the given conditions ($\alpha = 0.1$, $\frac{\rho_f}{\rho_g} \approx 1000$), the quality is very low (between 0.0001 and 0.0002, depending on the model used), the two phase friction multiplier does not exceed 1.2, so the two-phase friction pressure drop can be estimated by

$$\left(\frac{\partial p}{\partial z}\right)_{2\phi} \approx -760 \text{ N/m}^3 \tag{20}$$

For the bubble velocity, $v_g = v_f + v_r = \frac{G}{\rho_f(1-\alpha)} + v_r \approx 1.17$ m/s, and the given void fraction, Eq.(3.3-190) in Ref. 4 (with $\alpha_{fw} = \alpha_f$ and $\alpha_{gw} = \alpha_g$) yields

$$Z^2 = \frac{\lambda_f \rho_f v_f^2}{\lambda_g \rho_g v_g^2} \approx 510 \tag{21}$$

where λ_f and λ_g, respectively, are the liquid and gas friction factors, defined as shown on pp. 136 and 137 of Ref. 4.

Substituting this result into Eqs.(14) and (15), yields

$$(F_f^s)_{RELAP} = -\frac{\tau_f p_f}{A} = -(1-\alpha)\left(\frac{\partial p}{\partial z}\right)_{2\phi} \frac{Z^2}{\alpha + (1-\alpha)Z^2} = -0.9998\left(\frac{\partial p}{\partial z}\right)_{2\phi} = -759.8\,\mathrm{N/m^3} \tag{22}$$

$$(F_g^{Ind})_{RELAP} = -\frac{\tau_g p_g}{A} = -\alpha\left(\frac{\partial p}{\partial z}\right)_{2\phi} \frac{1}{\alpha + (1-\alpha)Z^2} = -0.0002\left(\frac{\partial p}{\partial z}\right)_{2\phi} = -0.2\,\mathrm{N/m^3} \tag{23}$$

At the same time, the actual partitioning of the wall shear between the liquid shear and the induced shear in the gas/vapor momentum equation is as follows

$$F_f^s = -(1-\alpha)\left(\frac{\partial p}{\partial z}\right)_{2\phi} = 684\,\mathrm{N/m^3} \tag{24}$$

$$F_g^{Ind} = -\alpha\left(\frac{\partial p}{\partial z}\right)_{2\phi} = 76\,\mathrm{N/m^3} \tag{25}$$

Comparing Eq.(22) with Eq.(24) and Eq.(23) with Eq.(25) one concludes that the RELAP5 prediction indicates that the gas phase practically does not contribute to the overall friction pressure drop, whereas the consistent two-fluid model shows that the presence of the gas phase introduces an additional irreversible pressure loss that is distributed between both phases according to their volumetric contributions.

The implications of this difference can be illustrated by rewriting Eqs.(5) and (6) with F^i given by Eq.(11)

$$-(1-\alpha)\frac{\partial p}{\partial z} - (1-\alpha)\rho_m g - F_f^s = 0 \tag{26}$$

$$-\alpha\frac{\partial p}{\partial z} - \alpha\rho_m g - F_g^{Ind} = 0 \tag{27}$$

Using the REPAP5/MOD3.3 results, $(F_f^s)_{RELAP} \approx -\left(\frac{\partial p}{\partial z}\right)_{2\phi}$ and $(F_g^{Ind})_{RELAP} \approx 0$, so that both Eq.(26) and Eq.(27) are satisfied only if

$$\frac{\partial p}{\partial z} \approx -\rho_m g \quad \text{and} \quad F_f^s \approx 0 \tag{28}$$

which means, <u>incorrectly</u>, that the total two-phase flow pressure drop is only due to the effect of gravity.

It is interesting to notice that a similar inconsistency was observed before (see References 1 and 2 and the attached slides of my lecture at the MIT conference last June), although for a different situation and flow conditions (horizontal flow in a micro-channel). In that case, the model typically used by the existing CFD codes produced completely unphysical results according to which the dispersed-phase (and relatively heavy) particles accelerated to a velocity significantly higher than the velocity of the liquid that was driving the particles. After the necessary corrections were made in the NPHASE code, the results turned out to be perfectly consistent. So, the problem is quite fundamental ann should be dealt with in a thorough manner.

The apparent inconsistency of the RELAP/MOD3.3 model can be briefly explained as follows:

- The analysis of a multidimensional two-fluid model shows that the increased pressure drop is due to the interfacial shear distributed over the entire flow area, not just at the wall. In particular, this term is not related to gas friction factor at the wall. Actually, for most dispersed bubbly flows, the effect of bubbles touching the wall is practically negligible.
- On the contrary, the approach used in RELAP/MOD3.3 is based on a very old concept (the reference papers were published in 1949 and 1967), that was developed at the time when the knowledge of the physics of two- and multiphase flows was very limited. Thus, several assumptions (such as the use of gas friction factor for dispersed bubbly flows in which bubbles are treated as rigid "particles" and the actual gas velocity field, which determines the shear stress, is not modeled at all) are purely artificial and, for some conditions, lead to unrealistic results.

The fact that the overall RELAP5/MOD3.3 predictions for reactor systems compare reasonably well with experimental data for which the code has been tested, may be explained by several reasons, one of which is that if the effect of wall friction is small compared to that of gravity, the modeling inconsistency discussed here may have a relatively small impact compared to other modeling uncertainties. Naturally, the availability of tuning knobs, that is inherent to all system codes, makes it more difficult to track the effects (and consistency) of individual modeling assumptions. Nevertheless, the present simple example shows that the wall friction partitioning model in RELAP5/MOD3.3 should be revisited, carefully checked and corrected as necessary.

2. Possible extension to multicomponent flows

As shown in References 1 and 2, the two-fluid model discussed in Section 1 can be readily extended to multiple fields. For application in nuclear reactor thermal-hydraulics and safety, such extension would allow for a mechanistically-based (but still contingent upon the availability of appropriate closure laws) treatment of two-phase flows with multiple size bubbles (e.g. large Taylor bubbles and small dispersed bubbles in slug flows), or multicomponent flows (consisting of liquid, vapor and noncondensables).

Specifically, assuming that the flow includes a single continuous field (liquid) and N dispersed fields (vapor/steam bubbles of different sizes and/or gas components) the generalized form of Eqs.(5) and (6) is

$$-\alpha_f \frac{\partial p}{\partial z} - \alpha_f \rho_f g - F_f^s + \sum_{k=1}^{N} F_k^i = 0 \tag{29}$$

$$-\alpha_{g,k}\frac{\partial p}{\partial z}-\alpha_{g,k}\rho_{g,k}g-F_{g,k}^{Ind}-F_k^i = 0 \tag{30}$$

where $k = 1,..., N$, $\alpha_{g,k}$ is the volumetric concentration of field-k, and α_f is the concentration of the liquid phase/field, that satisfies the following condition

$$\alpha_f = 1-\sum_{k=1}^{N}\alpha_{g,k} \tag{31}$$

The term, F_k^i in Eqs.(29) and (30) defines the interfacial force between the continuous field and dispersed field-k.

Eq.(29) and (30) can be rearranged, to obtain

$$F_{g,k}^{Ind} = \frac{\alpha_{g,k}}{\alpha_f}F_f^s-F_k^i+\alpha_f(\rho_f-\rho_{g,k})g \tag{32}$$

$$-\frac{\partial p}{\partial z}-\rho_m g-F_w^s = 0 \tag{33}$$

where

$$F_w^s = F_f^s+\sum_{k=1}^{N}F_{g,k}^{Ind} = -\left(\frac{\partial p}{\partial z}\right)_{2\phi} \tag{34}$$

is the total two-phase friction pressure gradient, and

$$\rho_m = \rho_f(1-\alpha_f)+\sum_{k=1}^{N}\rho_{g,k}\alpha_{g,k} \tag{35}$$

is the mixture density.

As can be seen, the structure of the multifield model is very similar to that of the two-field (two-fluid) model discussed before. Thus, its implementation in RELAP5/MOD3 seems to be feasible without any major restructuring of the code. I anticipate that a similar conclusion extends to the TRAC and MACE-M codes.

REFERENCES

1. Podowski, M.Z., "Modeling of Two-Phase Flows and Heat Transfer; Remarks on Recent Advancements and Future Needs", Keynote paper, Proc. 3rd Int. Conference Transport Phenomena in Multiphase Systems, Kielce, Poland, 2002.
2. Tiwari, P., Antal, S.P. and Podowski, M.Z., "On the Modeling of Dispersed Particulate Flows using a Multifield Model", in Computational Solids and Fluids Mechanics 2003 (ed. K.J. Bathe), Elsevier Science LTD, 2003 (also, see the keynote lecture slides).
3. Podowski, M.Z., "On the Development of Multidimensional Mechanistic Models of Multiphase Flows", 5th International Conference on Multiphase Flow, ICMF'04, Yokohama, Japan, May 30–June 4, 2004 (to be published).
4. RELAP5/MOD3.3 CODE MANUAL, Vol.1, NUREG/CR-5535/Rev.1, December, 2001.

On the modeling of dispersed particulate flows using a multifield model

Prashant Tiwari, Steven P. Antal, Michael Z. Podowski *

Center for Multiphase Research, Rensselaer Polytechnic Institute, 110, 8th Street, Troy, NY 12180, USA

Abstract

This paper is concerned with selected computational and modeling issues arising from using a multifield modeling framework to perform CFD simulations of multiphase flows. An approach is proposed to resolve an apparent multifield modeling inconsistency via an induced shear-stress correction term. The implementation is discussed of this correction term and other convergence improving algorithms into the NPHASE solver. The results of model testing are shown for dispersed particulate flows in a variety of geometries such as straight pipes, a U-bend and a helical tube.

Keywords: Two-phase particle flow; Multifield model; U-bend and helical microchannels

1. Overview of multifield model

In the multifield model, the governing conservation equations are determined with respect to a physical and computational domain, and include various interfacial effects between the fields. Specifically, the mass, momentum and energy conservation equations, respectively, for field k can be written as [1,2]

Mass:

$$\frac{\partial(\alpha_k\rho_k)}{\partial t}+\nabla\cdot(\alpha_k\rho_k\bar{\mathbf{v}}_k)=\Gamma_k+\sum_{n\in\aleph}\bar{m}''_{kn} \tag{1}$$

Momentum:

$$\begin{aligned}\frac{(\alpha_k\rho_k\bar{\mathbf{v}}_k)}{\partial t}&+\nabla\cdot(\alpha_k\rho_k\bar{\mathbf{v}}_k\bar{\mathbf{v}}_k)=-\alpha_k\nabla\bar{p}_k-(\bar{p}_k-\bar{p}_{ki})\nabla\alpha_k\\&+\nabla\cdot\alpha_k\left(\underline{\underline{\tau}}_k+\underline{\underline{\tau}}_k^{Re}\right)+\alpha_k\rho_k\underline{g}+\mathbf{F}_k+\Gamma_k\left(\mathbf{v}_m^I-\mathbf{v}_k^I\right)\\&+\sum_{n\in\aleph}\bar{m}''_{kn}\left(\mathbf{v}_n^I-\mathbf{v}_k^I\right)\end{aligned} \tag{2}$$

Energy:

$$\begin{aligned}\frac{(\alpha_k\rho_k\bar{e}_k)}{\partial t}&+\nabla\cdot\alpha_k\rho_k\bar{e}_k\bar{\mathbf{v}}_k)=\nabla\cdot\alpha_k\left[\left(-\bar{p}_k\underline{\underline{I}}_k+\underline{\underline{\tau}}_k+\underline{\underline{\tau}}_k^{Re}\right)\cdot\bar{\mathbf{v}}_k\right]\\&-\nabla\cdot\alpha_k\left(\mathbf{q}_k''+\mathbf{q}_k''^{Re}\right)+q''_{ik}\\&+\alpha_k\rho_k\mathbf{g}\cdot\bar{\mathbf{v}}_k+\Gamma_k\left[\bar{e}_{ik}+\tfrac{1}{2}\left(\mathbf{v}_m^I-\mathbf{v}_k^I\right)^2\right]+\sum_{n\in\aleph}\bar{m}''_{kn}\left(\mathbf{v}_n^I-\mathbf{v}_k^I\right)\end{aligned} \tag{3}$$

The model given by Eqs. (1)–(3) is a generalization of the well-established two-fluid model. The individual fields may represent either separate fluids and phases, or geometrically/structurally distinct flow configurations

Nomenclature

t	time
$\bar{m}''_{kn}$	interfacial mass transfer from field n into field k
$\bar{\mathbf{v}}_{ik}^n$	velocity of field n at the interface
$\aleph\ni k,n$	phase indicator
A'''	interfacial area density
C	model coefficient
F_c^S	shear force per unit volume continuous fields
$\underline{g}$	acceleration of gravity vector
$\bar{p}$	pressure
Re	Reynolds number
F_c	geometric correction factor
$\bar{\mathbf{v}}_k$	velocity vector of field k

Greek letters

α	volume fraction
ρ	fluid density
Γ	mass transfer rate
μ	fluid viscosity
τ	shear stress

Subscripts

c	continuous phase
d	dispersed phase

* Corresponding author. Tel.: +1 (518) 276-4000; Fax: +1 (518) 276-3055; E-mail: podowm@rpi.edu

© 2003 Published by Elsevier Science Ltd.
Computational Fluid and Solid Mechanics 2003
K.J. Bathe (Editor)

within a given physical fluid or phase. Examples include: continuous liquid field, dispersed small bubbles or particles, large (deformed) bubbles or bubble clusters, continuous gas/vapor field, and dispersed liquid field (droplets). For a typical dispersed two-phase two-field model the index, k, includes: cl – continuous liquid phase, and dv – dispersed vapor phase. On the other hand, for a four-field model, the following fields can be used: continuous liquid phase (cl), dispersed liquid (dl), continuous vapor (cv) and dispersed vapor (dv).

Several additional conditions, or closure laws, are needed to complete the model given by Eqs. (1)–(3). In general, the specific closure laws are flow-regime dependent. The form of individual interfacial closure laws depends on the specific physical phenomena. For example, for dispersed (with small size "particles") flows, the total interfacial force is given as a superposition of terms describing various effects [3]. The range of applications (limitations) and accuracy of predictions of the multifield model strongly depend on the degree to which the closure laws, determined in terms of ensemble-averaged state variables are capable of capturing the most important local mass, momentum and heat transfer phenomena.

2. Consistency of multifield model formulation

Although the multifield conservation equations seem to be a direct extension of those governing single-phase flows, it turns out that the averaging procedure introduced several constraints on the formulation of individual models. In particular, any constitutive laws used to close the model must be invariant, i.e., independent of the frame of reference (system of coordinates) or objective [3]. Another interesting constraint arising from the multifield modeling concept imposes a coupling effect between the continuous and disperse fields. Specifically, the effect discussed in this section is concerned with a shear stress induced by the continuous field (or fields) on the dispersed fields.

Let us consider a developing steady two-phase flow of diluted particles dispersed in a continuous fluid in a horizontal pipe. As the flow gradually reaches a fully developed pattern, particles will be moving in the axial direction with constant velocities. Consequently, the net force (in the axial direction – a combination of the drag and virtual mass forces) will approach zero, and so will the relative velocity of particles with respect to the continuous field. However, computer simulations using a two-field/two-fluid model typically show a positive relative velocity, the magnitude of which may vary from very small to significant, depending on the geometry and flow conditions. Naturally, such results are unphysical. This apparent inconsistency of the two- and, in general, multifield model formulation, and a method to resolve the problem, are discussed below. Since the flow (if any) inside the dispersed particles is normally not modeled by multifield models, when fully developed conditions are approached, the momentum equations for the continuous and any of the N-dispersed fields, respectively become

$$-(1-\langle\alpha\rangle)\frac{\partial p}{\partial z}-(1-\langle\alpha\rangle)\rho_c g_z - \sum_{i=1}^{N} F^{D}_{cd_i,z} - \sum_{i=1}^{N} F^{VM}_{cd_i,xz} - F^{S}_{c} = 0 \tag{4}$$

$$-\langle\alpha_{d,i}\rangle\frac{\partial p}{\partial z}-\langle\alpha_{d,i}\rangle\rho_{d,i}g_z + F^{D}_{cd_i,z} + F^{VM}_{cd_i,z} = 0 \tag{5}$$

where $\langle\alpha\rangle = \sum_{i=1}^{N}\langle\alpha_{d_i}\rangle$ and the virtual mass and drag forces, respectively, are given by

$$F^{VM}_{cd_i,z} = -C_{vm}\langle\alpha\rangle\rho_c\left[\left(\frac{\partial u_{d_i}}{\partial t}+u_{d_i}\frac{\partial u_{d_i}}{\partial z}\right)-\left(\frac{\partial u_c}{\partial t}+u_c\frac{\partial u_c}{\partial z}\right)\right] \tag{6}$$

$$F^{D}_{cd_i,z} = -\tfrac{1}{8}C_D\rho_c|u_{d_i}-u_c|(u_{d_i}-u_c)A^{in}_{d_i} \tag{7}$$

As can be seen, at fully developed conditions, the virtual mass force approaches zero and the axial pressure gradient becomes constant, $\partial p/\partial z = \text{constant}$. Thus, Eqs. (4) and (5) reduce to

$$F^{D}_{cd_i,z} = \langle\alpha_{d,i}\rangle\left[(\rho_m-\rho_{d,i})g_z + F^{S}_{c}\right] \tag{8}$$

In particular, for zero-gravity (on neutrally buoyant particles) the above result incorrectly implies at fully-developed conditions that $F^{D}_{cd_i,z} > 0$ and therefore, $|u_{d_i}-u_c| > 0$.

On the other hand, a force balance for the ith dispersed particle field is

$$\rho_{d,i}\frac{\mathrm{d}\mathbf{v}_{p,i}}{\mathrm{d}t} = (\rho_m-\rho_{d,i})\mathbf{g} - \frac{1}{V_{p,i}}(\mathbf{F}^{D}_{p,i}+\mathbf{F}^{VM}_{p,i}) \tag{9}$$

For fully developed flows, Eq. (9) yields

$$F^{D}_{c,d_i,z} = (\rho_m-\rho_{d,i})g_z \tag{10}$$

As can be readily shown, in order to obtain a consistent fully developed model formulation, an induced-shear force, $F^{IS}_{d_i}$, should be added to each dispersed-field momentum equation

$$-\langle\alpha_{d,i}\rangle\frac{\partial p}{\partial z}-\langle\alpha_{d,i}\rangle\rho_{d,i}g_z + F^{D}_{cd_i,z} + F^{VM}_{cd_i,z} - F^{IS}_{d_i} = 0 \tag{11}$$

given by

$$F^{IS}_{d_i} = \frac{\langle\alpha_{d,i}\rangle}{1-\langle\alpha_{d,i}\rangle}F^{S}_{c} \tag{12}$$

Thus, one concludes that although the friction pressure drop is entirely due to continuous field shear stress, the multiphase model formulation requires that a induced shear term be added to dispersed-field equations. The implementation of this shear-induced term into a CFD solver is discussed in the next section.

3. Overview of the NPHASE computer code

NPHASE [4,5] is a segregated, nominally pressure-based finite volume CFD code. Individual scalar transport equations are solved for momentum, energy and turbulence quantities for each field. Mixture and field continuity equations are solved in coupled or uncoupled fashions, using frozen coefficient linearizations. The code is fully unstructured and utilizes second-order accurate convection and diffusion discretizations. A key feature of NPHASE is that from the outset the software design has focused on the development of a reliable solver for multiphase flows. Also, the various interactions between the individual fields have been incorporated as an inherent part of the solution algorithm.

Key features of NPHASE include the following:

- Use of unstructured grids with arbitrary element types
- Capability to model an arbitrary number of fields (fluid components and/or phases)
- Built-in mechanistic modeling, integrated with numerics
- Improved robustness and numerical convergence

The use of unstructured meshes has several advantages over multiblock structured approaches, including: rapid grid generation, ability to generate quality meshes for complex geometries, economy of elements and more forthcoming adaptive refinement. Furthermore, hybrid unstructured topologies allow prism or hexahedron elements to be used near solid boundaries for high quality meshes in boundary layer regions, while accommodating transition to pyramids and tetrahedra in the core flow.

Front end software provides interfacing with multiblock structured meshes and, more generally, with unstructured meshes through the FIELDVIEW [6] unstructured data format. Grid generators that have been used to date in NPHASE simulations included Gridpro [7] for multiblock structured grids and Gridgen [8] to build hybrid meshes and specify boundary conditions. Accurate predictions of multiphase flows can only be made if the overall CFD algorithm limits the numerical error in the calculation. For the particle flows under consideration here, it was necessary to improve the so-called Rhie–Chow [9] velocity interpolation used to evaluate the velocity on the face of each control volume. The Rhie–Chow velocity interpolation is performed according to

$$U_{\text{face}} = \overline{U} + B_{\text{vel}}(\overline{\nabla p} - \nabla p) \tag{13}$$

where the over-bar represents averaged quantities from the neighboring nodes. For multiphase flow calculations the pressure gradient terms ($\overline{\nabla p}$ and ∇p) are significantly influenced by the hydrostatic pressure field. In many applications, the hydrostatic pressure field can vary in a highly non-uniform manner. Since the Rhie–Chow velocity interpolation includes pressure gradient terms, a non-uniform hydrostatic pressure field can introduce numerical errors in the predicted facial velocity. To minimize this effect, the standard Rhie–Chow velocity interpolation is modified as:

$$U_{\text{face}} = \overline{U} + B_{\text{vel}}\left([\overline{\nabla p - \rho_m g}] - [\nabla p - \rho_m g]\right) \tag{14}$$

The existing experience clearly shows that two-phase simulations can be very difficult to converge without this modification. In particular, this effect was found to be significant for particle flows when the effect of gravity was normal to the main flow direction. Another computational issue important for the class of problems mentioned above is associated with the numerical implementation of the induced shear term in the dispersed particle momentum equations. To implement the correction term in Eq. (12), the shear force is written as

$$F_d^{IS} = \frac{\langle \alpha_d \rangle}{1 - \langle \alpha_d \rangle} \nabla \cdot (\alpha_c \tau_c) \tag{15}$$

Normally, the shear stress tensor is treated implicitly in the numerical method in order to improve robustness and convergence. However in a segregated algorithm the forces coupled to other phases are usually treated explicitly as source terms. This, in turn, can significantly impact the solver's performance. To improve the robustness, a shear stress term that could be treated implicitly in the numerical method was introduced. Using this technique, Eq. (15) was modified as:

$$F_d^{IS} = \{\nabla \cdot (\alpha_d \tau_d)\}_{\text{implicit}} + \left\{ \frac{\langle \alpha_d \rangle}{1 - \langle \alpha_d \rangle} \nabla \cdot (\alpha_c \tau_c) - \nabla \cdot (\alpha_d \tau_d) \right\}_{\text{source term}} \tag{16}$$

Note that, at convergence this additional shear stress term does not effect the solution (the implicit and source term components cancel out). However, using this modified equation was found to improve the overall convergence characteristics of the solver.

4. Results

The results shown in this section have two objectives. The first objective, illustrated in Figs. 1 and 2, is to demonstrate the importance of the induced shear term for the accuracy of micro-size dispersed particle flow predictions using a multifield model. The second objective is to show the results of NPHASE simulations for particulate flows in complex geometries (Figs. 3 and 4).

Fig. 1 shows the results of calculations for a particulate flow in a straight horizontal pipe obtained using a standard two-fluid formulation (i.e., without the induced-shear term). The velocity distribution shown in this figure refers to the outlet section of the pipe where the flow is fully developed. Fig. 1a shows the radial velocity profiles for continuous liquid and dispersed particles (at an average volume fraction of 0.2). Although for the given kinematic equilibrium conditions between the fields, the velocity of particles at any radial location should be identical to the corresponding local liquid velocity of liquid, it can be readily seen

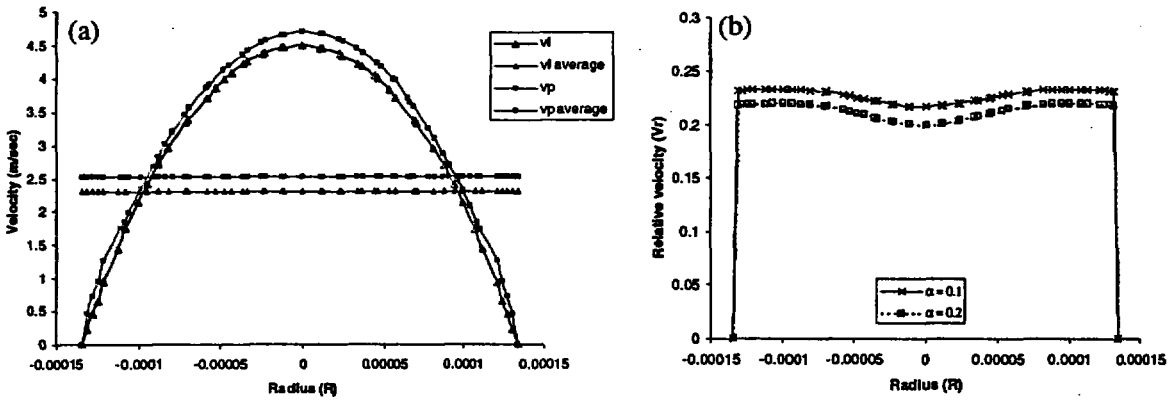

Fig. 1. (a) Radial liquid (vl) and particle (vp) velocity profiles near outlet of a straight pipe predicted by the original multifield model with an average inlet particle volume fraction, $\alpha = 0.2$. (b) Relative velocity ($vr = vp - vl$) across the pipe near the pipe outlet for neutrally buoyant particles at two different inlet volume fractions: $\alpha = 0.1$ and $\alpha = 0.2$.

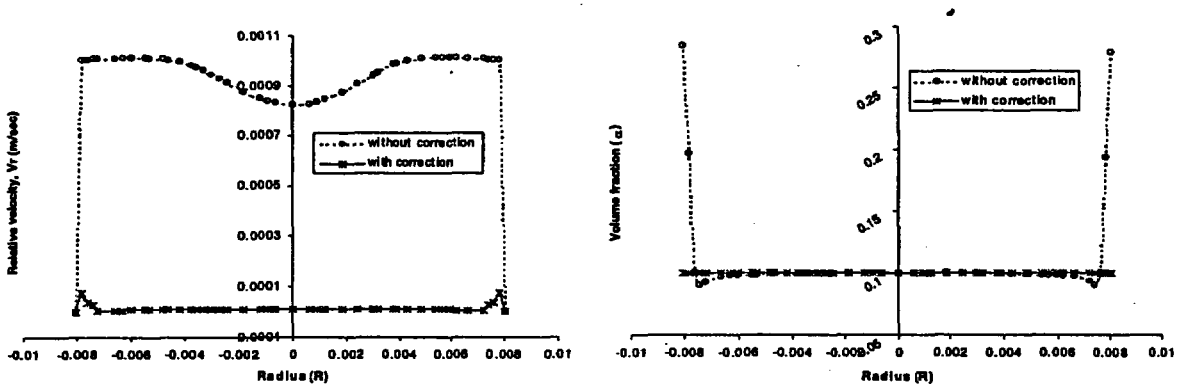

Fig. 2. Comparison of fully developed relative velocity and particle concentration with and without the induced-shear stress correction term. Calculations performed for neutrally buoyant particles using the NPHASE-code-based multifluid model: (left panel) relative velocity; (right panel) volume fraction.

that actually particles flow faster than the continuous liquid everywhere across the pipe. This physically inconsistent result is confirmed by the relative velocity calculations shown in Fig. 1b for two volumetric concentrations of particles. It is interesting to notice that the predictions error increases as the concentration of particles increases.

The effect of introducing the induced-shear correction terms is illustrated in Fig. 2. In these calculations, a 2 m long 1.6 cm ID straight pipe was used with an average liquid velocity of 0.154 m/s. Two different cases were analyzed in order to demonstrate the effect of the continuous-field-induced shear term.

The results obtained before and after incorporating the induced shear given by Eq. (12) are shown in Fig. 2. The inclusion of the correction term significantly reduces the relative velocity and improves the concentration prediction. Specifically, the predicted radial particle volume fraction becomes uniform and the relative velocity approaches zero everywhere across the pipe (including the near-wall region) as fully developed conditions are reached.

In order to demonstrate the consistency of NPHASE simulations, in addition to straight pipes, calculations were also performed for two types of complex geometries: a U-bend and a helical tube. For consistency of comparisons, the tube diameter in both cases was the same as for the straight pipe case discussed before.

The results for a U-bend are shown in Fig. 3. Comparing the velocity distributions at the entrance and exit of the curved section of the tube, one can identify the formation of curvature-induced Dean vortices [10]. The use of induced-shear correction term is also clearly seen in this figure, specifically, the predicted relative velocity with correction is almost at zero level. Local velocities at the next-to-wall node are always very difficult to converge and thus show a slight overshoot, but the predicted values (1e−5) are practically negligible.

The helix results are shown in Fig. 4. These results show a nearly uniform distribution of particles after incorporating the correction term in the particle momentum equation. Secondary flows due to Dean vortices are quite prominent

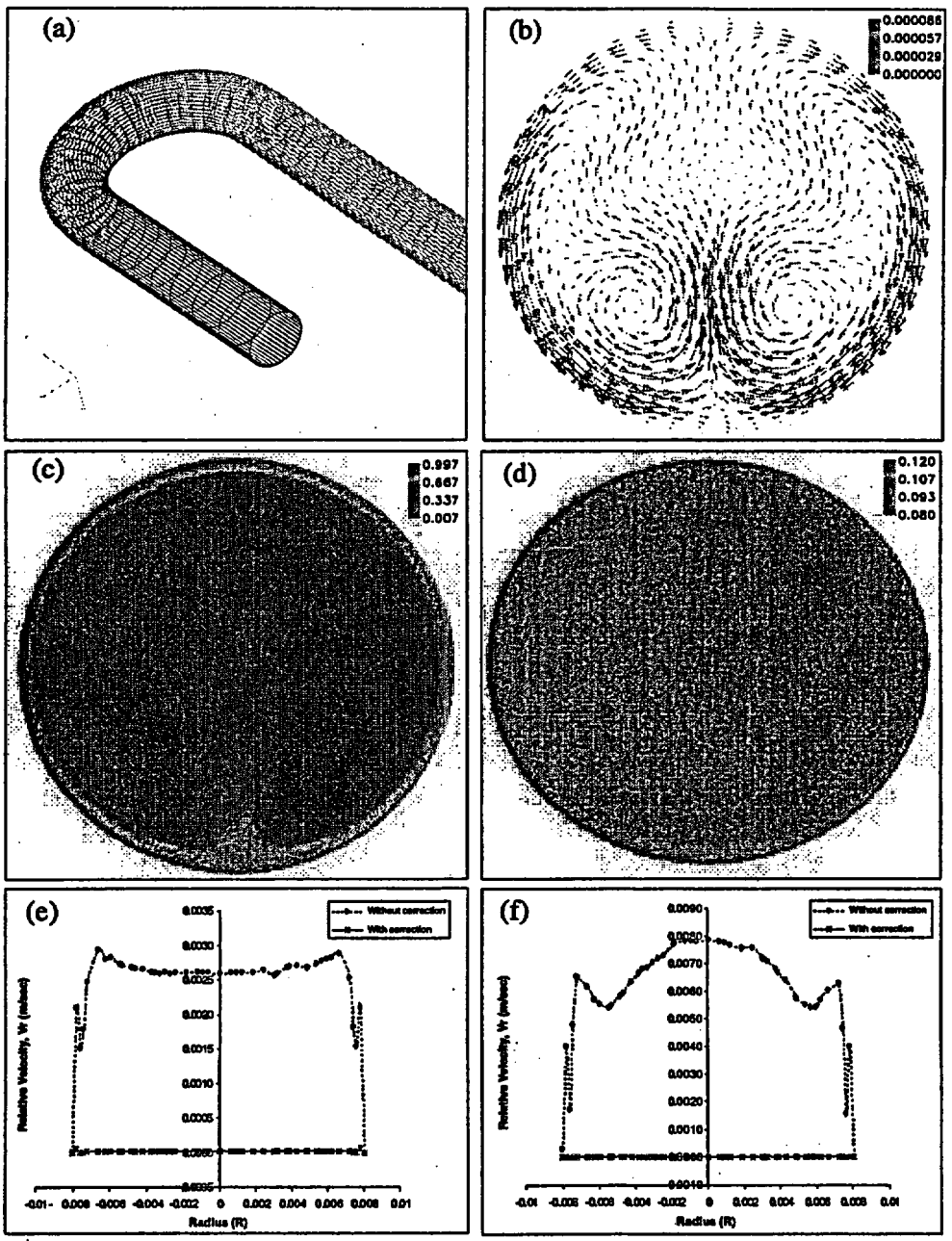

Fig. 3. Particle flow in a U-bend. (a) Mesh showing the U-bend region. (b) Secondary flow velocity vectors at the mid-section of U-bend; velocity vectors are colored with relative velocity (vr = vp − vl). (c) Volume fraction plot at the mid-section of the U-bend without using the correction term; notice the high volume fraction at the wall (~ 0.99). (d) Volume fraction at the mid-section of the U-bend with the correction term; predicted particle distribution is uniform in this case (max. ~ 1.002, min. ~ 0.099). (e) Relative velocities with and without the correction at the entry of the U-bend. (f) Relative velocities with and without the correction at the exit of the U-bend.

in this geometrical configuration. The importance of using a proper correction term is also shown in terms of both volume fraction and relative velocity distributions over the entire computational domain.

5. Conclusions

Selected computational and modeling issues were discussed associated with multidimensional simulations of

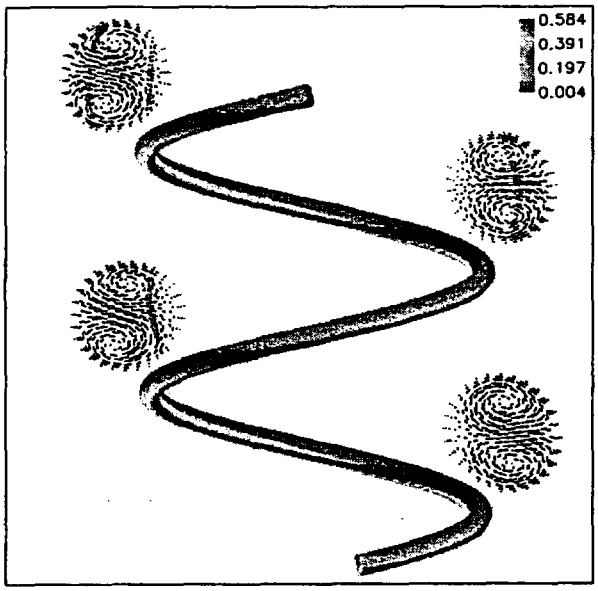

Fig. 4. Particle flow in a helical tube. The tube is colored with particle volume fraction on the tube surface. Also, secondary flows at various cross-sections of the tube are shown.

multiphase flows using a multifield modeling framework. An approach was proposed to resolve an apparent multifield modeling inconsistency via an induced shear-stress correction term. This correction was implemented in the NPHASE CFD solver and extensively tested. The results of NPHASE-based computer simulations show both modeling and computational consistency for a variety of geometries, including straight pipes, a U-bend and a helical tube.

References

[1] Antal SP, Podowski MZ, Lahey RT Jr. On the multidimensional modeling of annular two-phase flows around spacers. Proc 4th Int Conf Multiphase Flow, New Orleans, LA, 2001.
[2] Podowski MZ. Modeling of two-phase flow and heat transfer; remarks on recent advancements and future needs. Proc 3rd Int Conf Transport Phenomena in Multiphase Systems, Kielce, Poland, 2002.
[3] Drew DA. Analytical modeling of multiphase flows. In: Lahey Jr RT (Ed), Boiling Heat Transfer; Modern Developments and Advances. New York: Elsevier, 1992.
[4] Antal SP, Ettorre SM, Kunz RF, Podowski MZ. Development of a next generation computer code for the prediction of multicomponent multiphase flows. International Meeting on Trends in Numerical and Physical Modeling for Industrial Multiphase Flow, Cargese, France, 2000.
[5] Kunz RF, Yu WS, Antal SP, Ettorre SM. An unstructured two-fluid method based on the coupled phasic exchange algorithm. AIAA-2001-2672, 2001.
[6] FIELDVIEW 6 Reference Manual. Intelligent Light, 1999.
[7] Gridpro User Manual. Program Development Corp., 1998
[8] Gridgen User Manual, Version 13.3. Pointwise, 1999.
[9] Rhie CM, Chow WL. Numerical study of the turbulent flow past an airfoil with trailing edge separation. AIAA J. 1983;21.
[10] Dean WR. Fluid motion in curved channel. Proc R Soc London A 1928;121.

Rensselaer

Conference Paper

On the Modeling of Dispersed Particulate Flows using a Multifield Model

P. Tiwari, S. Antal and M.Z. Podowski
Center for Multiphase Research
Rensselaer Polytechnic Institute

Second MIT Conference on Computational Fluid and Solid Mechanics
Cambridge, Massachusetts, June 17-20, 2003

Center for Multiphase Research
Rensselaer Polytechnic Institute
CMR CMR CMR

Presentation/Lecture

On the Modeling of Two- and Multiphase Flows using a Multifield Model

Michael Z. Podowski

Center for Multiphase Research
Rensselaer Polytechnic Institute
CMR CMR CMR

Presentation Outline

- Introduction
- Multiscale aspects of multiphase flows
- Mechanistic Multidimensional Modeling of Multiphase Flow
- Modeling Dispersed Particulate Flows using a Multifield Model
- Conclusions

Center for Multiphase Research
Rensselaer Polytechnic Institute
CMR CMR CMR

Introduction

- Multiphase flows encompass a wide spectrum of phenomena, from nano to macro scales
- Applications include systems from very small (ultra-thin film technology and micro-channels) to very large (chemical systems, nuclear power reactors)

Center for Multiphase Research
Rensselaer Polytechnic Institute
CMR CMR CMR

Introduction (*continued*)

- Multiphase fluid mechanics and heat transfer can be investigated at several different scales and complexity levels
- In each case, a consistent model formulation and case-specific method(s) of analysis are critical issues

Center for Multiphase Research
Rensselaer Polytechnic Institute
CMR CMR CMR

Multiscale aspects of multiphase flows

Super-thin liquid film on inclined wall

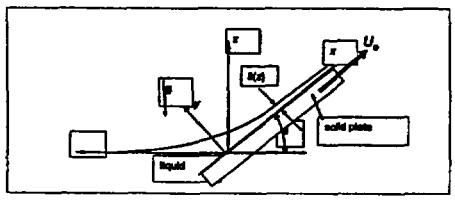

- Film momentum equation is $\frac{\partial \tau_{yz}}{\partial y} = -\frac{\partial(\sigma K + \Phi)}{\partial x} + \rho g_x$

where: $K = \frac{\delta''}{(1+\delta'^2)^{3/2}}$ $\Phi = \frac{B}{\delta''}$ ← *Hamaker constant*

Stationary film of fully-wetting liquid

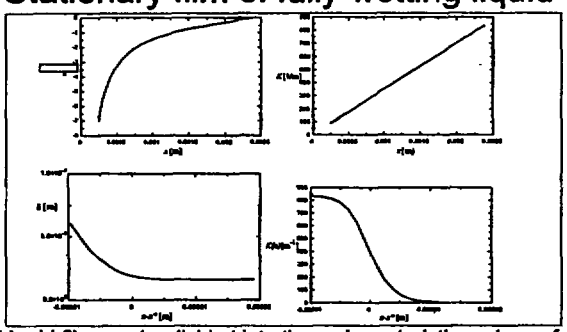

Liquid film can be divided into three characteristic regions of dramatically different scales: capillary, transition, nano

Super-thin liquid film on inclined wall

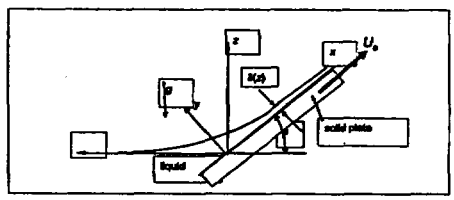

- Film momentum equation is $\frac{\partial \tau_{yz}}{\partial y} = -\frac{\partial(\sigma K + \Phi)}{\partial x} + \rho g_x$

where: $K = \frac{\delta''}{(1+\delta'^2)^{3/2}}$ $\Phi = \frac{B}{\delta''}$ ← *Hamaker constant*

Effect of wall velocity on thickness of moving film

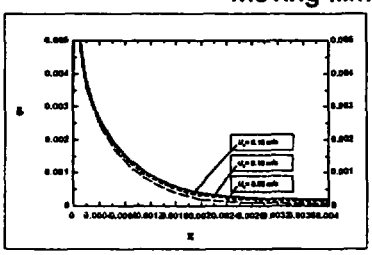

Liquid film profile

$$\Delta = \beta(Ca)^{\alpha}$$

where

$$Ca = \frac{\mu U_0}{\sigma}$$

$$\Delta = \frac{\delta_\infty}{a} = \delta_\infty \sqrt{\frac{\rho g}{\sigma}}$$

Simplified model (Probstein, 1994): $\Delta = 0.946(Ca)^{0.667}$

Complete flow model (Podowski & Kumbaro, 2003): $\Delta = 0.834(Ca)^{0.542}$

Long air bubble flowing in distilled water along inclined tube

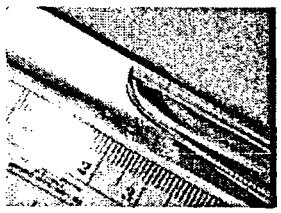

Clean inner tube surface (u_B=10 cm/s)

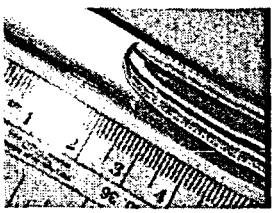

Nano-particle coated surface (u_B=8 cm/s)

Two-phase flow regimes in vertical pipes

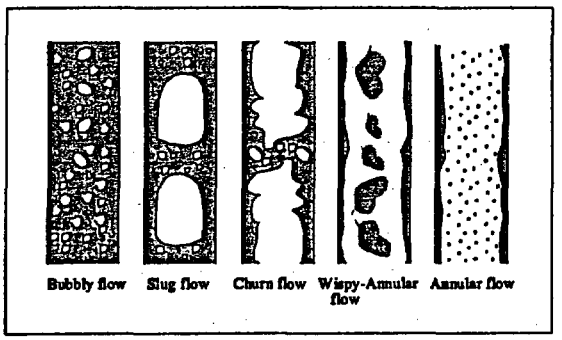

Mechanistic Multidimensional Modeling of Multiphase Flow

- Modeling concepts
  - Direct Numerical Simulations
  - Averaging concepts used to predict fluid/fluid interactions
    - Eulerian Framework
    - Eulerian-Lagrangian Framework

Interface tracking

- Instantaneous conservation equations
- Modeling of interfacial phenomena
  - Interface between two continuous phases/fluids
  - dispersed "particles"

3-D Predictions of Slug Flow (Anglart & Podowski, 2002)

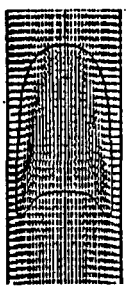

Flow inside and outside Taylor bubble

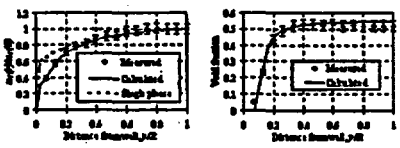

(a) velocity (b) void fraction

Radial distributions of reduced chord-averaged liquid velocity and void fraction in slug flow; j_l= 0.6 m/s, j_v = 0.22 m/s

Interface Between Two Continuous Fluids

- Velocity at interface $\mathbf{v}_{k,i} + \dot{m}''_{k,i}/\rho_k = \mathbf{v}_{l,i} + \dot{m}''_{l,i}/\rho_l = \mathbf{v}_i$
- Mass transfer at interface $\dot{m}''_{k,i} = -\dot{m}''_{k,i} = \left(q''_{k,i} + q''_{l,i}\right)/h_{fg}$
- Shear stress at interface $\tau_{k,i} = \tau_{l,i}$
- Surface momentum equation at interface

$$\nabla_s \cdot \{\underline{\underline{I}}[\sigma + (\kappa^s - \mu^s)\nabla_s \cdot \mathbf{v}^s]\} + \nabla_s \cdot \{\mu^s[\nabla_s \mathbf{v}^s \cdot \underline{\underline{I}} + \underline{\underline{I}} \cdot \nabla_s \mathbf{v}^{s^T}]\} = \mathbf{n}_s \cdot \left(-p\underline{\underline{I}} + \underline{\underline{\tau}}\right)\Big|_s$$

Multifield Conservation Equations

- Mass $$\frac{\partial \alpha_k \rho_k}{\partial t} + \nabla \cdot (\alpha_k \rho_k \overline{\mathbf{v}}_k) = \Gamma_k$$
- Momentum $$\frac{\partial (\alpha_k \rho_k \overline{\mathbf{v}}_k)}{\partial t} + \nabla \cdot (\alpha_k \rho_k \overline{\mathbf{v}}_k \overline{\mathbf{v}}_k) = -\alpha_k \nabla \overline{p}_k - (\overline{p}_k - \overline{p}_{ki})\nabla \alpha_k + \nabla \cdot \alpha_k \left(\underline{\underline{\overline{\tau}}}_k + \underline{\underline{\tau}}_k^{Re}\right) + \alpha_k \rho_k \mathbf{g} + \mathbf{M}_k$$
- Energy $$\frac{\partial (\alpha_k \rho_k \overline{e}_k)}{\partial t} + \nabla \cdot (\alpha_k \rho_k \overline{\mathbf{v}}_k \overline{e}_k) = -\nabla \cdot \left[\alpha_k \left(-\overline{p}_k \underline{\underline{I}} + \underline{\underline{\overline{\tau}}}_k + \underline{\underline{\tau}}_k^{Re}\right) \cdot \overline{\mathbf{v}}_k\right] - \nabla \cdot \left[\alpha_k \left(\overline{\mathbf{q}}''_k + \mathbf{q}''^{Re}_k\right)\right] + \alpha_k \rho_k \mathbf{g} \cdot \overline{\mathbf{v}}_k$$

Interfacial Source Terms

- Mass

$$\Gamma_k = -\frac{1}{\Delta t}\sum_{i\in[\Delta t]}\frac{1}{|\mathbf{v}_i\cdot\mathbf{n}_k|}\left[\rho_k(\mathbf{v}_k-\mathbf{v}_i)\cdot\mathbf{n}_k\right]+\sum_n m_{nk}^{\alpha}$$

- Momentum

$$\mathbf{M}_k = -\frac{1}{\Delta t}\sum_{i\in[\Delta t]}\frac{1}{|\mathbf{v}_i\cdot\mathbf{n}_k|}\left[\rho_k\mathbf{v}_k(\mathbf{v}_k-\mathbf{v}_i)+p_k\underline{\mathbf{I}}+\underline{\tau}_k\right]\cdot\mathbf{n}_k+\Gamma_{nk}(\mathbf{v}_n^i-\mathbf{v}_k^i)+\sum_n m_{nk}^{\alpha}(\mathbf{v}_n^i-\mathbf{v}_k^i)$$

- Energy

$$E_k = -\frac{1}{\Delta t}\sum_{i\in[\Delta t]}\frac{1}{|\mathbf{v}_i\cdot\mathbf{n}_k|}\left[\rho_k e_k(\mathbf{v}_k-\mathbf{v}_i)+\mathbf{q}_k^i\right]\cdot\mathbf{n}_k+\Gamma_{nk}\left[e_{kl}+\frac{1}{2}(\mathbf{v}_n^i-\mathbf{v}_k^i)^2\right]+\sum_n m_{nk}^{\alpha}(\mathbf{v}_n^i-\mathbf{v}_k^i)^2$$

Formulation of fluid/particle flow model

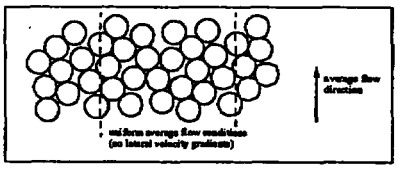

Case 1:

Packed particles

Particle motion (Lagrangean frame of reference)

$$\rho_p\frac{d\mathbf{v}_p}{dt}=\rho_p V_p\mathbf{g}+\mathbf{F}_{f\to p}-\mathbf{F}_{c\to p}$$

Averaged equations (Eulerian frame of reference)

$$\frac{\partial(\alpha_d\rho_d\overline{\mathbf{v}}_d)}{\partial t}+\nabla\cdot(\alpha_d\rho_d\overline{\mathbf{v}}_d\overline{\mathbf{v}}_d)=-\alpha_d\nabla\overline{p}_d-(\overline{p}_d-p_{dl})\nabla\alpha_d+\nabla\cdot\alpha_d\left(\underline{\overline{\tau}}_d+\underline{\tau}_d^{Re}\right)+\alpha_d\rho_d\mathbf{g}+\mathbf{M}_d$$

$$\frac{\partial(\alpha_c\rho_c\overline{\mathbf{v}}_c)}{\partial t}+\nabla\cdot(\alpha_c\rho_c\overline{\mathbf{v}}_c\overline{\mathbf{v}}_c)=-\alpha_c\nabla\overline{p}_c-(\overline{p}_c-p_{cl})\nabla\alpha_c+\nabla\cdot\alpha_c\left(\underline{\overline{\tau}}_c+\underline{\tau}_c^{Re}\right)+\alpha_c\rho_c\mathbf{g}+\mathbf{M}_c$$

Typical two-fluid formulation

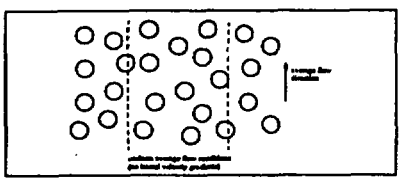

Case 2:

Dilute particles

Particle motion (Lagrangean frame of reference)

$$\rho_p\frac{d\mathbf{v}_p}{dt}=\rho_p V_p\mathbf{g}-\mathbf{F}_{c\to p}$$

Average equations (Eulerian frame of reference)

$$\frac{\partial(\alpha_d\rho_d\overline{\mathbf{v}}_d)}{\partial t}+\nabla\cdot(\alpha_d\rho_d\overline{\mathbf{v}}_d\overline{\mathbf{v}}_d)=p_{dl}\nabla\alpha_d+\alpha_d\rho_d\mathbf{g}+\mathbf{M}_d$$

$$\frac{\partial(\alpha_c\rho_c\overline{\mathbf{v}}_c)}{\partial t}+\nabla\cdot(\alpha_c\rho_c\overline{\mathbf{v}}_c\overline{\mathbf{v}}_c)=-\alpha_c\nabla\overline{p}_c-(\overline{p}_c-p_{cl})\nabla\alpha_c+\nabla\cdot\alpha_c\left(\underline{\overline{\tau}}_c+\underline{\tau}_c^{Re}\right)+\alpha_c\rho_c\mathbf{g}+\mathbf{M}_c$$

Dilute particles do not constitute a "field"

Practical approach to apparent modeling inconsistency: pseudo-two-fluid model

Corrected momentum conservation equation for dispersed particle "field"

$$\frac{\partial(\alpha_d\rho_d\overline{\mathbf{v}}_d)}{\partial t}+\nabla\cdot(\alpha_d\rho_d\overline{\mathbf{v}}_d\overline{\mathbf{v}}_d)=-\alpha_d\nabla\overline{p}_d-(\overline{p}_d-p_{dl})\nabla\alpha_d+\nabla\cdot\alpha_d\left(\underline{\overline{\tau}}_d+\underline{\tau}_d^{Re}\right)+\alpha_d\rho_d\mathbf{g}+\mathbf{M}_d+\mathbf{M}_{c\to d}^{IND}$$

where

$$\mathbf{M}_{c\to d}^{IND}\quad\left\{=\nabla(\alpha_d\overline{p}_d)\right\}$$

is the continuous-field-induced force

Modeling Dispersed Particulate Flows using a Multifield Model

All numerical simulations shown next were performed using an advanced CFD code, NPHASE

Analysis of the apparent Inconsistency of Multifield Model

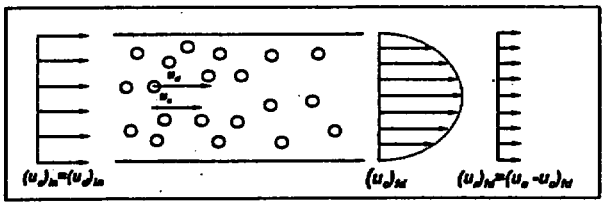

- Low concentration flow of dispersed particles:
  - drag force is the only interfacial force
  - particles are driven by the continuous phase

NPHASE Calculation for Fully-Developed Dispersed Particle Flow using Standard Two-Field Model

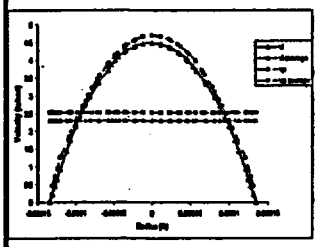

Radial liquid (v_l) and particle (v_p) velocity profiles

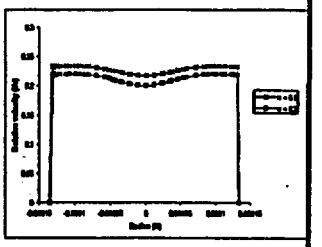

Relative velocity ($v_r = v_p - v_l$) across the pipe

Multifield Model of Dispersed Particle Flows

- Momentum equations (for fully-developed flow)

$$0=-\alpha_c\frac{\partial p_c}{\partial x}-\alpha_c\rho_c g_x+M^D_{d,x}-M^S_{c,x}$$

$$0=-\alpha_d\frac{\partial p_d}{\partial x}-\alpha_d\rho_d g_x-M^D_{d,x}$$

- Drag force can be obtained from (for any g_x)

$$\left|M^D_{d,x}\right|=\alpha_d\left|M^S_{c,x}+\alpha_c(\rho_c-\rho_d)g_x\right|$$

- For horizontal flows or neutrally buoyant particles

$$\boxed{\left|v_{r,x}\right|=\left|v_{d,x}-v_{c,x}\right|=2\sqrt{\frac{2}{C_D\rho_c}\frac{d_d}{6}\left|M^S_{c,x}\right|}>0}$$

Correction of Dispersed Phase Momentum Equation

- Force balance for an arbitrary particle

$$\rho_d\frac{dv_p}{dt}=(\rho_m-\rho_d)g-\frac{1}{V_p}F^D_p$$

yields $M^D_{d,x}=\alpha_d(\rho_m-\rho_d)g_x$

- Corrected momentum equation for dispersed fields includes a continuous-phase-induced force

$$0=-\alpha_d\frac{\partial p_d}{\partial x}-\alpha_d\rho_d g_x-M^D_{d,x}-M^H_{d,x}$$

where

$$\boxed{M^H_{d,x}=\frac{\alpha_d}{\alpha_c}M^S_{c,x}}$$

NPHASE Predictions for a U-Bend

Computational grid

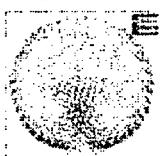

Dean Vortices

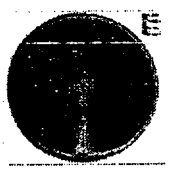

(a) before correction

Particle concentration

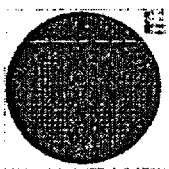

(b) after correction

Effect of Model Correction on Relative Particle Velocity for Fully-Developed Flow in U-Bend

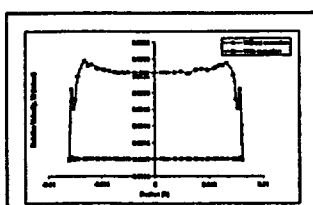

Inlet to the curved section

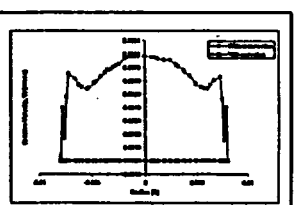

Exit of the curved section

NPHASE Predictions of velocity field and particle concentration at mid-section of a U-bend geometry

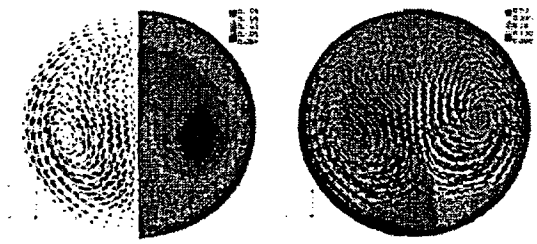

without gravity

with gravity

3-D simulation of particle flow in a helical micro-tube using corrected two-field model

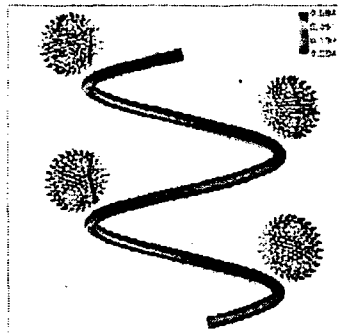

Summary and Conclusions

- Concepts of multidimensional modeling of two-phase flows have been presented
- Apparent inconsistency has been discussed of multifield model formulation for dilute particulate flows
- Predictive capabilities of the NPHASE CFD code have been demonstrated for particulate two-phase flows in complex geometries

Fourth International Conference "*Transport Phenomena in Multiphase Systems*", Baranow Sandomierski, Poland, June 24-27, 2002

MODELING OF TWO-PHASE FLOW AND HEAT TRANSFER; REMARKS ON RECENT ADVANCEMENTS AND FUTURE NEEDS

Michael Z. Podowski - Center for Multiphase Research, Rensselaer Polytechnic Institute, Troy, NY 12180, USA

ABSTRACT

Significant progress has been made in recent years in our understanding of the basic physics of two-phase flow and heat transfer. Nevertheless, the modeler still frequently faces situations where sources of experimental data and/or theoretical concepts are either very restrictive or even inconsistent with one another.

The objective of this paper is to discuss selected modeling and computational aspects of two-phase flow and heat transfer, including both recent advancements in the field and needs for additional work in order to enhance the truly mechanistic character of theoretical predictions. The following issues will be discussed: modeling concepts (instantaneous vs. averaged equations), consistency of averaging, formulation of local closure laws, and potential sources of physical and computational uncertainties.

Keywords: multiphase flow and heat transfer, multidimensional models, CFD

INTRODUCTION

It is evident that significant progress has been made in recent years in our understanding of the basic physics of two-phase flow and heat transfer, as well as in the predictive capabilities for two-phase systems and processes. In the latter case, a systematic trend has been observed that new mechanistically based models slowly but steadily replace the phenomenological models that have been widely used in this field for a long time. Nevertheless, due to the complexity of multiphase flow phenomena, both the experimental and analytical results are typically fragmented and case-specific, so that the modeler frequently faces situations where sources of experimental data and/or theoretical concepts are either very restrictive or even inconsistent with one another.

The objective of this paper is to discuss selected modeling and computational aspects of two-phase flow and heat transfer, with the emphasis given to two interrelated issues: (a) recent advancements in the field and, (b) needs for additional work in order to enhance the truly mechanistic character of theoretical predictions. The specific issues include: modeling concepts (instantaneous vs. averaged equations), the consistency of averaging and its impact on local closure laws, and potential sources of physical and computational uncertainties. Selected experimental and numerical results will be shown to illustrate the theoretical considerations of both models and methods of analysis.

1. PHYSICAL MODELS OF MULTIPHASE FLOW AND HEAT TRANSFER

Any combination of non-mixing fluids (or phases) moving inside a given volume can be described by local instantaneous conservation equations for mass, momentum and energy. Assuming that the k-th (k=1,2,...) component of the multifluid flow can be modeled using the concept of continuum, the corresponding Eulerian conservation equations for mass, momentum and energy, respectively, become

$$\frac{\partial \rho_k}{\partial t} + \nabla \cdot (\rho_k \mathbf{v}_k) = 0 \tag{1}$$

$$\frac{\partial (\rho_k \mathbf{v}_k)}{\partial t} + \nabla \cdot (\rho_k \mathbf{v}_k \mathbf{v}_k) = -\nabla p_k + \nabla \cdot \underline{\underline{\tau}}_k + \rho_k \mathbf{g} \tag{2}$$

$$\frac{\partial (\rho_k e_k)}{\partial t} + \nabla \cdot (\rho_k \mathbf{v}_k e_k) = -\nabla \cdot \mathbf{q}_k'' + \nabla \cdot \left[\left(-p_k \underline{\underline{\mathbf{I}}} + \underline{\underline{\tau}}_k \right) \cdot \mathbf{v}_k \right] + \rho_k \mathbf{g} \cdot \mathbf{v}_k \tag{3}$$

For any k, these equations are valid only at locations that pertain to fluid-k at a given time instant. At the boundaries between the fluids or phases (which may vary with time), appropriate boundary conditions must be formulated, such as those for the continuity of velocity, shear stress and heat flux. Note that if the interfaces are being modeled as sharp discontinuities in fluid density and other properties, parameters such as pressure and velocity and temperature gradients, may also experience discontinuity.

In the case of dilute particle suspensions or fluids containing surfactants, the bulk flow model must be complemented by an appropriate surface dynamics model, consisting of the surface momentum equation combined with the surface equation of state used to evaluate the particle transport toward and/or away from the free surface. The surface momentum equation can be written as [1]

$$\nabla_s \cdot \{ \underline{\underline{\mathbf{I}}}_s [\sigma + (\kappa^s - \mu^s) \nabla_s \cdot \mathbf{v}^o] \} + \nabla_s \cdot \{ \mu^s [\nabla_s \mathbf{v}^o \cdot \underline{\underline{\mathbf{I}}}_s + \underline{\underline{\mathbf{I}}}_s \cdot \nabla_s \mathbf{v}^{o^T}] \} = \mathbf{n}_s \cdot \left(-p \underline{\underline{\mathbf{I}}} + \underline{\underline{\tau}} \right) \Big|_s \tag{4}$$

where σ is the surface tension, μ^s and κ^s, respectively are the interfacial shear and dilatational viscosities, $\mathbf{v}^o$ is the surface velocity vector, and $\mathbf{n}_s \cdot \left(-p \underline{\underline{\mathbf{I}}} + \underline{\underline{\tau}} \right) \Big|_s$ is the

effective momentum transfer into the interface due to the different bulk pressure/shear tensors at each side of the interface.

The surface concentration of dispersed "particles" can be obtained from a proper isotherm as a function of the bulk concentration near the interface. One way to determine the bulk distribution of "particles", especially for very small size particles, is via the advection-diffusion equation. An alternative approach, applicable to small dispersed gas bubbles, liquid droplets of solid particles), is to use a Lagrangian frame of reference according to which the motion of a "particle" is given by the Newton's second law

$$\frac{d\left(m_p \mathbf{v}_p\right)}{dt} = V_p\left(\rho_m - \rho_p\right)\mathbf{g} - \mathbf{F}_p \tag{5}$$

In such case, the flow inside bubbles or droplets is normally ignored, so that the instantaneous mass and energy of the "particle" are determined based on the interfacial transfers of the respective quantities

$$\frac{dm_p}{dt} = \int_{A_p} \rho_c\left(\mathbf{v}_c - \mathbf{v}_p\right)\cdot \mathbf{n}\, dA_p \tag{6}$$

$$\frac{d(m_p e_p)}{dt} = \int_{A_p} \left[\rho_c e_c\left(\mathbf{v}_c - \mathbf{v}_p\right) + \mathbf{q}''_{i,c}\right]\cdot \mathbf{n}\, dA_p \tag{7}$$

2. FIRST PRINCIPLE COMPUTATION MODELING OF MULTIPHASE FLOWS

The analytical and/or computational difficulties associated with accurate predictions of multiphase flow and heat transfer are mainly in the modeling of interfaces the shape and position of which changes with time. Several numerical methods have been developed to solve the instantaneous local flow equations over the entire multiphase flow domain. These methods include, but are not limited to, the volume of fluid (VOF) method, the level set (LS) method and the Second Gradient (SG) method. Other methods, such as the front tracking (FT) method, have also been used to study two-phase flows.

The basic concept in the VOF method [2] is the introduction of a transport equation

$$\frac{\partial F}{\partial t} + \mathbf{v}\cdot\nabla F = 0 \tag{8}$$

where $0 \le F(\mathbf{x}, t) \le 1$ represents the volumetric concentration of a selected fluid.

According to the definition, those cells for which $0 < F < 1$, contain the interface. In addition, the normal direction to the surface is indicated as the direction along

which F changes most rapidly. The flow velocity vector, $\mathbf{v}(\mathbf{x},t)$, is found by solving simultaneously the momentum and mass conservation equations for the fluid over the entire computational domain. The effect of surface tension is accounted for by adding a pseudo-body force given by, $B_\sigma = \sigma K \nabla F / (\Delta F)$, where ΔF is the local jump of F across the transition region, and $K = -\nabla \cdot (\nabla F / |\nabla F|)$ is the interface curvature. One of the advantages of the VOF method is that is can be applied to a large spectrum of computational grids, including simple rectangular structured grids. For a given F, the location of the interface in individual computational cells is determined from the gradients of F. Eq.(8) normally requires a special numerical treatment (reconstruction procedure) to avoid a smearing of the step (or rapidly changing) function F, and to obtain a locally-smooth interface. In order to conserve the mass of the fluids at both sides of the interface, the integrated volume of evolving structures, such as bubbles or droplets, is adjusted at the end of each time step. Knowing the shape of the interface, the updated values of F in those cells that contain the interface are calculated from geometric considerations.

In the Level Set (LS) formulation [3], a level function, ϕ is defined in such a way that $\phi = 0$ anywhere on the interface, $\phi(\mathbf{x},t)$ satisfies Eq.(8) over the entire computational domain, and it is used to determine the local fluid properties (density and viscosity) as

$$\eta(\mathbf{x}) = \eta_j + (\eta_k - \eta_j) H_\varepsilon(\phi(\mathbf{x})) \tag{9}$$

where H_ε is the Heaviside function given by

$$H_\varepsilon(a) = \begin{cases} 0 & \text{if } a < -\varepsilon \\ 0.5 + a/(2\varepsilon) + [\sin(\pi a/\varepsilon)]/2\pi & \text{if } |a| \le \varepsilon \\ 1 & \text{if } a > \varepsilon \end{cases} \tag{10}$$

and ε is the prescribed "thickness" of the interface. Consequently, ϕ is a measure of the distance between the interface and a point on either side of the interface (including the side information). The effect of surface tension in the LS method is accounted for similarly as in the VOF method.

An important difference between the VOF and LS methods is that the latter method uniquely determines the position of the interface (at $\phi = 0$), so that no reconstruction procedure is needed. However, the conservation of mass is a problem, since artificial fluid densities are associated with the numerical "thickness" of the interface.

Both the VOF and LS methods have been mainly used to incompressible flows without phase change. An attempt to apply the LS method to film boiling was made by Son & Dhir [4]. They modified Eq.(10) by replacing the fluid velocity by the

interfacial velocity $\mathbf{v}_i = \mathbf{v} + \dot{m}_i''/\rho$, where $\dot{m}_i'' = q_i''/h_{fg}$ is the interfacial mass flux due to phase change (boiling). Also, an extension of the VOF method to flows with phase change was proposed by Welch & Wilson [5].

Whereas the physical models behind the VOF and LS methods assume a discontinuity of fluid properties at the interface (or an infinitessimal thickness of the interface), both algorithms utilize an artificial (or numerical) thickness of the interface. On the other hand, the microscopic-level physics of the interfacial region clearly indicates that the molecular density of the fluid undergoing phase change from liquid to vapor (or vice versa) varies continuously across the phase change region. Using a generalized form of the fluid equations of motion that account for the 'internal capilarity', Jamet et al. [6] developed a numerical approach called the Second Gradient (SG) method. One of the major computational issues associated with the SG approach is concerned with resolving the transition of fluid properties across an interface the thickness of which is of the order of Å, while maintaining a reasonable-size discretization.

In general, first principle numerical simulations (FPNS), also referred to as direct numerical simulations (DNS), of two-phase flows are computing intensive, so they are often applied to two-dimensional problems. An illustration of full three-dimensional simulations of slug flows using the VOF method is given in Figures 1 and 2. Figure 1 shows the predicted shape and liquid (water) velocity field outside, and gas (air) velocity field inside, a Taylor bubble in a vertical cylindrical pipe. The velocity vectors are shown using stationary and moving (with the bubble) systems of coordinates. As can be seen, flow reversal occurs in the liquid film outside the Taylor bubble, whereas acceleration is observed in the liquid slug behind the bubble. This, in turn, leads to the formation of secondary azimuthal flows. As it was shown by Anglart & Podowski [8], the resultant flow asymmetry and wake formation may affect the interaction between Taylor bubbles in slug flows, possibly leading to bubble coalescence.

Figure 2 presents radial profiles of local pressure at different axial locations along the pipe. The results show that the predicted radial pressure distributions both inside and outside the Taylor bubble are almost uniform, except for small perturbations in the tail section of the bubble. In particular, the pressure on each side of the bubble surface is practically the same (within the range of numerical accuracy) as the average pressure of the corresponding fluid. The pressure drop across the interface, although distributed over a final thickness rather than a sudden change, agrees well with the Young-Laplace equation.

It is interesting to notice that the axial pressure distribution at any radial location basically is a repeating pattern of an almost constant pressure inside Taylor bubbles (the effects of gravity and shear in the gas are minimal), followed by a gradual drop in the liquid slug region. This is schematically shown in Figure 3, where the average pressure drop for a fully-developed annular flow is also shown.

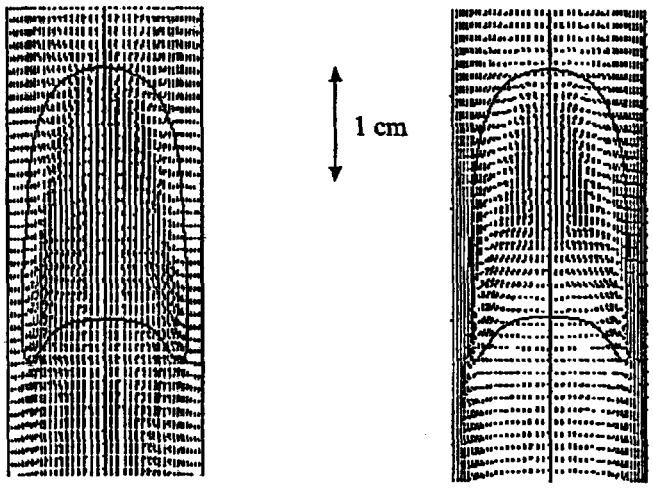

(a) stationary system of reference (b) system moving with the bubble

Figure 1. A 3-D prediction of velocity field and Taylor bubble shape in air/water slug flow using the VOF method, according to Anglart & Podowski [7].

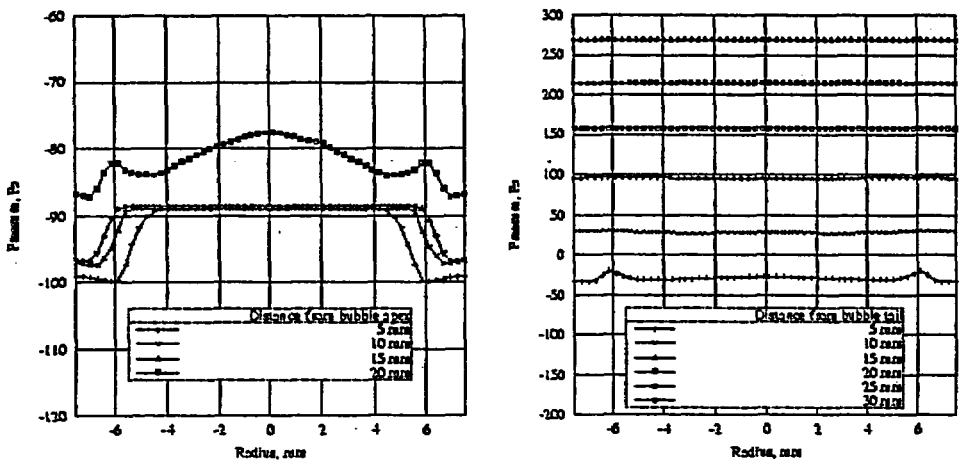

(a) (b)

Figure 2. Radial distributions of pressure for the flow field shown in Figure 1 [7]: (a) - in the bubble region, (b) - in the liquid slug region.

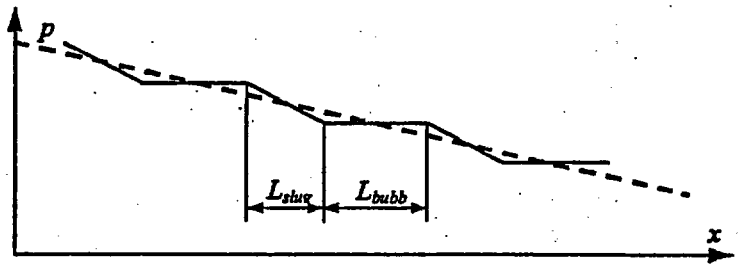

Figure 3. A schematic of the axial pressure distribution in fully-developed slug flows.

3. MULTIFIELD MODEL

The conservation equations, Eq.(1)-(3), describe fluid mechanics both inside and outside gas/vapor bubbles. Theoretically, they can be used to track the motion of individual bubbles, droplets or particles in multifluid multiphase flows in a rigorous deterministic manner. Practically, most multiphase flows involve probabilistic factors and the governing phenomena are characterized by statistical distributions. Since tracking individual bubbles in two or multiphase flows is normally neither practical nor necessary to understand flow characteristics, the modeling concept based on temporal, spatial and statistical (ensemble) averaging may prove very useful in analyzing complex situations involving multiphase flow and heat transfer.

As an illustration, let us consider a typical form of conservation equations for mass, momentum and energy, respectively, obtained by applying the appropriate averaging procedure to Eqs. (1)-(3)

$$\frac{\partial \alpha_k \rho_k}{\partial t} + \nabla \cdot (\alpha_k \rho_k \bar{\mathbf{v}}_k) = \Gamma_k \tag{11}$$

$$\begin{aligned} &\frac{\partial (\alpha_k \rho_k \bar{\mathbf{v}}_k)}{\partial t} + \nabla \cdot (\alpha_k \rho_k \bar{\mathbf{v}}_k \bar{\mathbf{v}}_k) = -\alpha_k \nabla \bar{p}_k - (\bar{p}_k - \bar{p}_{ki}) \nabla \alpha_k \\ &+ \nabla \cdot \alpha_k \left(\underline{\underline{\tau}}_k + \underline{\underline{\tau}}_k^{Re} \right) + \alpha_k \rho_k \mathbf{g} + \mathbf{M}_k \end{aligned} \tag{12}$$

$$\begin{aligned} &\frac{\partial (\alpha_k \rho_k \bar{e}_k)}{\partial t} + \nabla \cdot (\alpha_k \rho_k \bar{\mathbf{v}}_k \bar{e}_k) = -\nabla \cdot \left[\alpha_k \left(-\bar{p}_k \underline{\underline{\mathbf{I}}} + \underline{\underline{\tau}}_k + \underline{\underline{\tau}}_k^{Re} \right) \cdot \bar{\mathbf{v}}_k \right] \\ &- \nabla \cdot \left[\alpha_k \left(\bar{\mathbf{q}}_k'' + \mathbf{q}_k''^{Re} \right) \right] + \alpha_k \rho_k \mathbf{g} \cdot \bar{\mathbf{v}}_k + E_k \end{aligned} \tag{13}$$

where $\underline{\underline{\tau}}_k^{Re}$ is the turbulent shear stress, $\mathbf{q}_k''^{Re}$ is the turbulent heat flux, and the corresponding interfacial source terms for fluid-k are given by

$$\Gamma_k = -\frac{1}{\Delta t} \sum_{i \in [\Delta t]} \frac{1}{|\mathbf{v}_i \cdot \mathbf{n}_k|} \left[\rho_k (\mathbf{v}_k - \mathbf{v}_i) \cdot \mathbf{n}_k \right] \tag{14}$$

$$\mathbf{M}_k = -\frac{1}{\Delta t}\sum_{i\in[\Delta t]}\frac{1}{|\mathbf{v}_i\cdot\mathbf{n}_k|}\left[\rho_k\mathbf{v}_k(\mathbf{v}_k-\mathbf{v}_i)+p_k\underline{\underline{\mathbf{I}}}+\underline{\underline{\tau}}_k\right]\cdot\mathbf{n}_k+\Gamma_{mk}\left(\mathbf{v}_m^i-\mathbf{v}_k^i\right) \tag{15}$$

$$E_k = -\frac{1}{\Delta t}\sum_{i\in[\Delta t]}\frac{1}{|\mathbf{v}_i\cdot\mathbf{n}_k|}\left[\rho_k e_k(\mathbf{v}_k-\mathbf{v}_i)+\mathbf{q}_{i,k}''\right]\cdot\mathbf{n}_k+\Gamma_{mk}\left[e_{ki}+\frac{1}{2}\left(\mathbf{v}_m^i-\mathbf{v}_k^i\right)^2\right] \tag{16}$$

The model given by Eqs.(14)-(16) has been derived for gas-liquid two-phase flows with well defined topology. Specifically, it applies to dispersed bubbly flows where the interfacial interactions occur across bubble/liquid interfaces that gradually evolve in time and space. However, in the case where the interfacial interactions occur within a given phase, e.g., between dispersed liquid droplets and a liquid film, or as a result of bubble coalescence or breakup, the ensemble-averaged conservation equations, Eqs.(14)-(16), must be complemented by additional terms. This, in turn, leads to the formulation of a multifield model of multiphase flows. In this model, which is a generalization of the well-established two-fluid model, the individual fields may represent either separate fluids and phases, or geometrically/topologically distinct flow configurations within a given physical fluid or phase. Examples include: continuous liquid field, dispersed small bubbles or particles, large (deformed) bubbles or bubble clusters, continuous gas/vapor field, and dispersed liquid field (droplets).

In the multifield model, the governing conservation equations are determined with respect to a common physical and computational domain, and include terms accounting for the various interfacial effects between the individual fields. Specifically, the interfacial source terms in Eqs.(11), (12) and (13), respectively, must be expanded by adding the following terms: $\sum_n \dot{m}_{nk}''$, $\sum_n \dot{m}_{nk}''\left(\mathbf{v}_n^i-\mathbf{v}_k^i\right)$, $\sum_n \dot{m}_{nk}''\left(\mathbf{v}_n^i-\mathbf{v}_k^i\right)^2$, where $\dot{m}_{nk}''$ is the interfacial mass transfer from field-*n* into field-*k*, both representing the same phase.

For a typical two-phase two-field model the index, *k*, includes: *cl* - continuous liquid phase, and *dv* - dispersed vapor phase. On the other hand, for a four-field model, the following fields can be used: continuous liquid phase (*cl*), dispersed liquid (*dl*), continuous vapor (*cv*) and dispersed vapor (*dv*).

Several additional conditions, or closure laws, are needed to close the model given by Eqs.(11)-(16). The form of individual interfacial closure laws depends on the specific physical phenomena. For example, for dispersed (with small size "particles") flows [9], the total interfacial force is given as a superposition of terms describing various effects ($\mathbf{M}_k=\mathbf{M}_k^D+\mathbf{M}_k^L+\mathbf{M}_k^{VM}+\mathbf{M}_k^{TD}+\ldots$). The range of applications (limitations) and accuracy of predictions of the multifield model strongly depend on the degree to which the closure laws, determined in terms of ensemble-averaged state variables (such as $\alpha_k, \overline{\mathbf{v}}_k, \overline{e}_k, \overline{p}_k$) are capable of capturing the most important (for a given situation) local mass, momentum and heat transfer phenomena. Selected issues arising from the multifield model formulation are discussed in the next section.

4. ISSUES ARISING FROM THE MULTIFIELD MODEL

4.1. Induced Effect of Coupling between Continuous and Disperse Fields

Consider a developing two-phase flow of diluted particles dispersed in a continuous fluid in a horizontal pipe, with a drag force being the only interfacial force (see Figure 4).

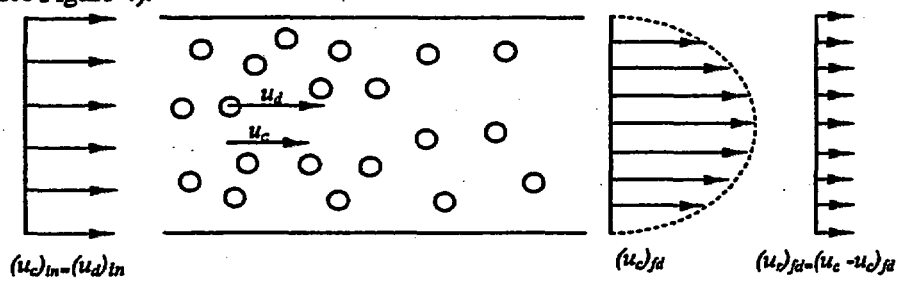

Figure 4. A schematic of developing dispersed two-phase flow.

For a given flow rate of the continuous field and any assumed velocity distribution at the inlet to the pipe, the flow of dispersed particles is governed by the drag force only. Thus, as the flow gradually reaches a fully-developed pattern, particles will be moving in the axial direction with a constant velocity. Consequently, the net force (actually, the drag force only) will approach zero and so will the relative velocity of particles. Actually, computer simulations using a typical two-fluid model will always show a positive relative velocity, the magnitude of which may vary from very small to significant, depending on the geometry and flow conditions. This apparent inconsistency of the two- and, in general, multifield model formulation is discussed below.

Since the flow inside dispersed particles (if any) is not modeled, the fully-developed momentum equations for the continuous and any of the N_d-dispersed fields, respectively become

$$0=-(1-\alpha)\frac{\partial \overline{p}_c}{\partial x}-(1-\alpha)\rho_c g_x+\sum_{j=1}^{N_d} M^D_{d,j,x}-M^S_{c,x} \tag{17}$$

$$0=-\alpha_{d,j}\frac{\partial \overline{p}_{d,j}}{\partial x}-\alpha_{d,j}\rho_{d,j}g_x-M^D_{d,j,x} \tag{18}$$

where $\alpha=1-\sum_{i=1}^{N_d}\alpha_{d,j}$ is the volume fraction of the continuous field. Since for fully-devoloped flows, $\partial\overline{p}_c/\partial x=\partial\overline{p}_{d,j}/\partial x=\partial\overline{p}/\partial x=constant$, combining Eqs.(17) and (18) yields

$$M^{D}_{d,i,x} = \alpha_{d,i} M^{S}_{c,x} > 0 \tag{19}$$

Eq.(19) implies that $v_{r,i,x} = v_{d,i,x} - v_{c,x} = 2\sqrt{\frac{2}{C_D \rho_c} \frac{d_{d,i}}{6\alpha_{d,i}} M^{D}_{d,i,x}} > 0$.

On the other hand, the force balance for a single particle that belongs to the i-th field is

$$\rho_{d,i} \frac{d\mathbf{v}_{p,i}}{dt} = (\rho_m - \rho_{d,i})\mathbf{g} - \frac{1}{V_{p,i}} \mathbf{F}^{D}_{p,i} \tag{20}$$

For a fully-developed flow, Eq.(20) yields

$$M^{D}_{d,i,x} = \alpha_{d,i} (\rho_m - \rho_{d,i}) g_x \tag{21}$$

Replacing Eq.(18) by

$$0 = -\alpha_{d,i} \frac{\partial \overline{p}_{d,i}}{\partial x} - \alpha_{d,i} \rho_{d,i} g_x - M^{D}_{d,i,x} - M^{IS}_{d,i,x} \tag{22}$$

where $M^{IS}_{d,i,x}$ is the averaging-induced shear force on the i-th dispersed field, and combinig Eq.(21) with Eqs.(17) and (22), the following expression is deduced

$$M^{IS}_{d,i,x} = \frac{\alpha_{d,i}}{1-\alpha} M^{S}_{c,x} \tag{23}$$

Hence, if the induced-shear force is added to each of the dispersed-field momentum equations, the overall model will properly predict the relative velocity in fully-developed flows.

4.2. Averaging for Slug Flow Regime

In non-dispersed two-phase flows, the shape of interface is normally a part of the solution. In the case of slug flows the kinematic closure laws can be conveniently deduced from the first-principle simulations discussed in Section 2, using the chord averaging concept illustrated in Figure 5(a). Specifically, the total interfacial force on field-k can be expressed as [7]

$$\mathbf{M}_k = \mathbf{M}_k^{static} + \mathbf{M}_k^{dynamic} + \mathbf{M}_k^{excess} = \mathbf{M}_k^{form} + \mathbf{M}_k^{shear} \tag{24}$$

It can be shown that, unlike for dispersed flows, $\mathbf{M}_l \neq \mathbf{M}_v$. It can also be shown that for gas/liquid flow the interfacial shear is negligible, and the major forces in the

axial and radial directions, responsible for the velocity and void distributions (see Figure 5) are [7]:

$$M_x^D = \frac{1}{2}\frac{C_D}{L_C}\rho_l\left\{\left[\overline{u}_l(0)-\overline{u}_l(r_B)\right]^2-\left[\overline{u}_l(0)-\overline{u}_l(r)\right]^2\right\} \tag{25}$$

$$M_{l,r}^{static} = -(\rho_l-\rho_v)gL_C\alpha_v\frac{d\alpha}{dr} \tag{26}$$

$$M_{l,y}^{dynamic} = \frac{1}{2}\frac{C_L}{L_C}\rho_l\left\{\left[\overline{u}_l(0)-\overline{u}_l(r_B)\right]^2-\left[\overline{u}_l(0)-\overline{u}_l(r)\right]^2\right\}\frac{d\alpha}{dr} \tag{27}$$

where $C_L = C_D = 20$ and $M_{l,y}^{static} + M_{l,y}^{dynamic} \cong 0$.

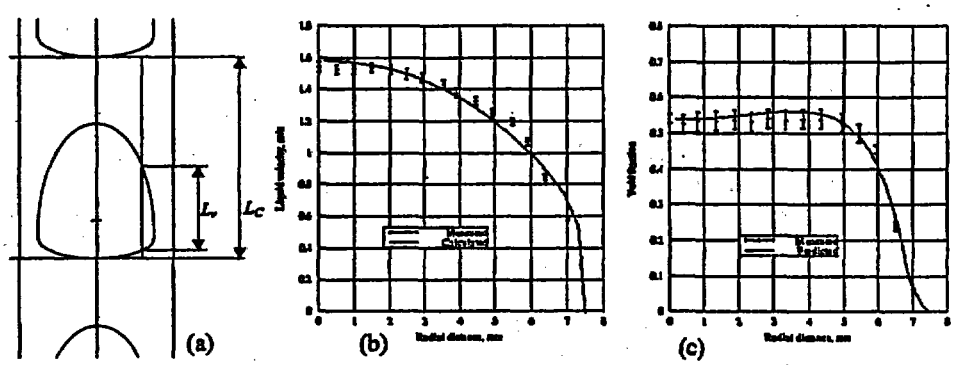

Figure 5. Two-fluid simulations of slug flows [7]: (a) averaging concept, (b) predicted and measured radial liquid velocity, (c) predicted and measured radial void distribution.

Another important closure law that can be deduced from the first-principle simulations is the bubble-induced turbulent shear. This bubble-shape induced term appears in the averaged momentum equation, Eq.(12), even if the actual flow is laminar, and can be quantified [7] via a pseudo-turbulennt viscosity, $\mu^{Bt} = \rho_l l^2 \left|\partial\overline{u}_l/\partial r\right|$, where the bubble-induced mixing length is given by $l = 2\langle\alpha\rangle R\left[(1-r/R)^2+(1-r/R)^4\right]$.

4.3. Averaging in the Presence of Thin Films

Multiphase flows are frequently accompanied by the formation of thin liquid films. As an example, a typical geometry of gas/liquid two-phase annular flow is shown in Figure 6. In such cases, details of flow inside the film cannot be resolved because of either the film thickness being comparable to, or smaller than, the computational grid

used in the simulations, or since the wavy film surface, governed by small-scale phenomena (turbulence), is smoothed out as a result of averaging.

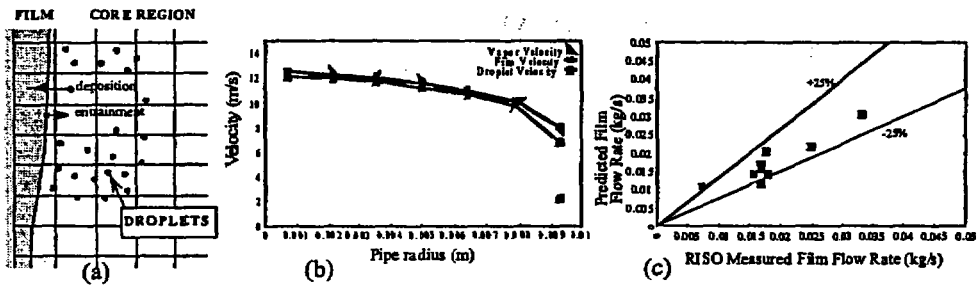

Figure 6. Application of multifield model to annular flows: (a) illustration of a 3-Field model, (b) radial velocity profiles in a pipe predicted by Antal & al. [10], (c) predicted vs. measured film flow rate on the inner rod in an annulus [11].

Whereas the three-dimensional distributions of the gas and dispersed droplet fields in annular flows can be readily modeled by a multifield model given by Eqs.(11)-(13), the liquid film is normally modeled by using the average film thickness and the axial and azimuthal velocities as state variables. The resultant mass and momentum conservation equations, respectively become

$$\rho_l\left[\frac{\partial\delta_{lf}}{\partial t}+\frac{\partial(\delta_{lf}\bar{u}_{lf,x})}{\partial x}+\frac{\partial(\delta_{lf}\bar{u}_{lf,z})}{\partial z}\right]=\dot{m}_d''-\dot{m}_e''-\Gamma_{lf}\delta_{lf} \tag{28}$$

$$\rho_l\left[\frac{\partial(\delta_{lf}\bar{u}_{lf,x})}{\partial t}+\frac{\partial(\delta_{lf}\bar{u}^2_{lf,x})}{\partial x}+\frac{\partial(\delta_{lf}\bar{u}_{lf,x}\bar{u}_{lf,z})}{\partial z}\right]=-\delta_{lf}\frac{\partial\bar{p}}{\partial x}-\tau_w+\tau_i \tag{29}$$

$$-\rho_l g\delta_{lf}+F_{lf}^d-F_{lf}^e-F_{lf}^\Gamma-F_{lf}^{disj}$$

Naturally, Eqs.(28) and (29) apply only to the near wall region where the liquid film field is present. Furthermore, the overall model requires that additional closure laws (for the deposition ($\dot{m}_d''$) and entrainment ($\dot{m}_e''$) rates, film evaporation rate (Γ_{lf}), the corresponding momentum transfer terms ($F_{lf}^d, F_{lf}^e, F_{lf}^\Gamma$), and wall and interfacial shear (τ_w and τ_i)) be formulated in terms of local state variables for all three fields. In the case of super-thin films, Eq.(29) also accounts for the effect of disjoining pressure (F_{lf}^{disj}). Nevertheless, once such closure laws are formulated, the overall model is capable of predicting various annular flow situations of practical interest, such as [9, 10]: developing flows (see Figure 6(b)), flows in heated channels, flows in pipes with central rods (where two films form, one on each the inner and outer surface, see Figure 6(c)), and flow around local obstacles (e.g., spacers in rod bundles).

4.4. Forced-Convection Boiling

An interesting application of the multifield model is concerned with forced convection subcooled (or low quality) boiling. As shown in Figure 7, bubbles formed in high heat flux subcooled boiling get crowded neat the heated wall and then quickly collapse. Thus, unlike in adiabatic two-phase flows, where kinematic forces such as lift, lubrication and turbulent dispersion are mainly responsible for the local void fraction across the channel, the lateral bubble transport and distribution in the present case are mainly driven by the nucleation-induced force pushing the newly formed bubbles away from the wall and by the effect of bubble condensation in contact with subcooled liquid. Naturally, the above mentioned nucleation force, which in turn results in a nucleation-rate-dependent bubble velocity at the wall, becomes important only at high local void fractions.

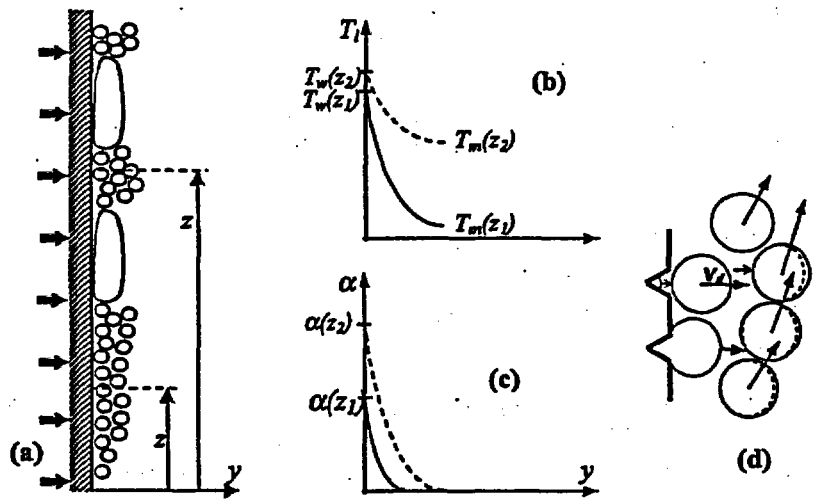

Figure 7. An illustration of high heat flux subcooled boiling at pre-CHF conditions: (a) bubble formation along the heated wall, (b) lateral temperature distribution, (c) lateral void fraction, (d) nucleation-induced force pushing dispersed bubbles away from the wall.

A sample result of predictions by Podowski & Antal [12] using a three-field model that accounts for this effect is shown in Figure 8. The three fields included: continuous liquid, dispersed bubbles and elongated bubbles forming at the wall due to bubble coalescence. The effect of elongated bubbles on local heat transfer conditions

has been quantified by partitioning the heated surface into the portion subjected to dispersed-bubble nucleate boiling (A''_{nb} is the corresponding wall area fracton) and that along the elongated bubble

$$\overline{q}''_w = \overline{q}''_{nb} A''_{nb} + \left[\overline{q}''_{ls} \frac{L_{ls}}{L_{lb}} + \overline{q}''_{dry} \left(1 - \frac{L_{ls}}{L_{lb}} \right) \right] (1 - A''_{nb}) \tag{30}$$

where $\overline{q}''_{ls}$ is the heat flux along the part of the elongated bubbles that is separated from the wall by an evaporating thin liquid film (the corresponding area fraction is $(1 - A''_{nb}) L_{ls} / L_{lb}$, where L_{ls} is the length of the liquid sublayer), and $\overline{q}''_{dry} \ll \overline{q}''_{ls}$ is the heat flux along the part that is in direct contact with the wall following partial film evaporation.

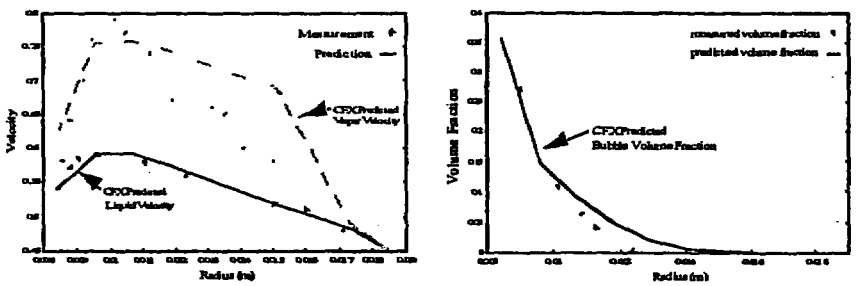

Figure 8. A comparison [12] between the predicted and measured [13] local distributions of velocity and void fraction in forced convection subcooled boiling.

Since the heat removed from the wall in the elongated bubble region is mainly due to heat conduction across, and the subsequently evaporation of, a thin liquid film, as the concentration of long bubbles increases, more heat must transferred to the cooolant in the gradually shrinking dispersed bubble region. Consequently, the wall temperature and the concentration of small bubbles start increasing, to eventually prevent liquid replenishment at the wall and cause wall temperature excursion (CHF). The predictions by the overall model are shown in Table 1.

Predictions of CHF reported in the literature are typically characterized by considerable (15-30%) errors. Several reasons can be identified to explain those inaccuracies. Typically, they include experimental uncertainties and the complex local multiphase flow patterns and modes of heat transfer. However, it also important to account for the possible effect of solid surface on bubble size, shape and motion. As an illustration, the geometry and flow conditions of long air bubbles in an inclined pipe filled with distilled water are shown in Figure 9. The pipe geometry and

material, and the bubble size, are identical in both cases. However, the bubble in Figure 9(a) is in direct contact with the wall, whereas the one in Figure 9(b) is separated from the wall by a thin (10-20 μm) liquid film. As a result of different shapes and wall shears, the bubble velocity was different for each case; specifically, the velocity of the bubble in Figure 9(b) was almost 20% higher. The only reason for that was that the result in Figure 9(a) was obtained for a clean surface of the pipe, whereas in the other case the surface was coated with a tiny layer of nanoparticles. Needless to say, if specific boiling experiments were performed for the same conditions, but using heaters characterized by different surface properties (such as wettability), the measured boiling heat transfer in general, and CHF in particular, would likely experience some systematic differences.

Table 1.
CFD Predictions of CHF [12] compared against the data of Saito et al. [14]

Mass Flux (kg/m^2s)	Liquid Subcooling (K)	Predicted CHF (kW)	Measured CHF (kW)	Error of CHF Prediction [%]
512	30	241	241	2
512	20	172	211	16
1236	30	305	332	8

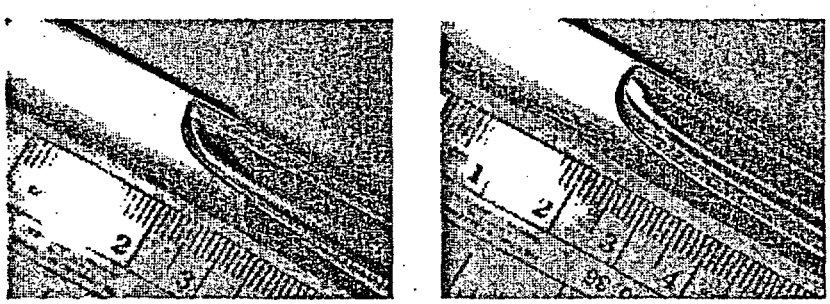

(a) clean inner tube surface (b) nano-particle coated tube surface

Figure 9. Long bubble flowing along an inclined tube.

5. COMMENTS ON EMERGING FUTURE ADVANCEMENTS

Whereas significant progress has already been made in the field of multiphase flow and heat transfer, the list of unresolved important issues is quite long. Examples of problems where future advancements are both needed and, arguably, within reach, are:

- Flow topology transition (bubble coalescence/breakup; size distribution; effect of bubble size, shape and concentration on flow stability; liquid film stability).

- Modeling of local phenomena in unstructured flow regimes (e.g. churn and wispy annular).
- Multiphase flows and heat transfer in complex geometries (impact of local phenomena, such as mixing/phase-separation and evaporation/condensation, on oscillations and instabilities).
- Turbulence in multiphase flows (wall and interface induced).
- Mechanistic modeling of boiling and CHF.
- Multiscale modeling, encompassing scales from molecular to continuum.
- Systematic qualification of experimental data, models and computational tools.

REFERENCES

1. Edwards, D.A., Brenner, H., and Wasan, D.T., *Interfacial Transport Processes and Rheology*, Butterworth-Heinemann, 1991
2. Hirt C.W. and Nichols B.D., *Volume of Fluid (VOF) Method for the Dynamics of Free Boundary, J. Comp. Phys.*, Vol. 39, 1981, pp. 201-225.
3. Osher S. and Sethian, J.A., *Fronts propagating with curvature-dependent speed: algorithms based on Hamilton-Jacobi formulation*, J. Comp. Phys. 79, 1988, pp.12-49
4. Son G. and Dhir V.K., *Numerical simulation of film boiling near critical pressures with a level set method*, J. HeatTransfer, Vol. 120, 1998, pp. 183-192
5. Welch S.W.J. and Wilson J., A volume of fluid based methodfor fluid flows with phase change, [, J. Comp. Phys., Vol. 160, 200, pp.662-775
6. Jamet D., Lebaigue O., Coutris N. and Delahye J.M., *The second gradient methos for the direct numerical simulatinof liquid-vapor flowswith phase change*, J. Comp. Phys., Vol. 169, 2001, pp.624-651
7. Anglart H. and Podowski M.Z., *On the multidimensional modeling of gas/liquid slug flows*, Proc. 12th Int. Heat Transfer Conf., Grenoble, France, August 18-23, 2002 (in print)
8. Anglart H. and Podowski M.Z., *Fluid mechanics of Taylor bubbles and slug flow in vertical channels*, Nuclear Science and Engineering, Vol. 140, No. 2, 2002, pp.165-171
9. Lahey R.T., Jr. and Drew D., *On the development of multidimensional two-fluid models for vapor/liquid two-phase flows*, Chem. Eng. Comm, Vol. 118, 1992, pp.125-139
10. Antal S.P., Kurul, N., Podowski M.Z. and Lahey R.T., Jr., *The Development of Multidimensional Modeling Capabilities for Annular Flows*, Proc 3th Int. Conf. on Multiphase Flow, Grenoble, France, 1998
11. Antal S.P., Podowski M.Z. and Lahey R.T., Jr., *On the multidimensional modeling of annular two-phase flows around spacers*, Proc 4th Int. Conf. on Multiphase Flow, New Orleans, LA, 2001
12. Podowski M.Z., and Antal S.P., *CFD* predictions *of temperature excursion (CHF) in low-quality boiling in heated channels*, Proc. 12th Int. Heat Transfer Conf., Grenoble, France, August 18-23, 2002 (in print)
13. Velidandla V., Putta S.P., Roy R.P. and Kaira S.P., *Velocity field in turbulent subcooled Boiling flow*, Proc. 30th National Heat Transfer Conference, Portland, OR, HTD-Vol. 314, No. 12, 1995
14. R. Hino and T. Ueda, *Studies on heat transfer and flow characteristics in subcooled flow boiling - Part 2: Flow characteristics*, Int. J. Multiphase Flow, Vol. 11, 1995, pp. 283-297